# New flavor physics in di- and trilepton events from single-top production at the LHC and beyond

Yoav Afik[1,*] Shaouly Bar-Shalom,[1,†] Amarjit Soni,[2,‡] and Jose Wudka[3,§]

[1]*Physics Department, Technion–Institute of Technology, Haifa 3200003, Israel*
[2]*Physics Department, Brookhaven National Laboratory, Upton, New York 11973, USA*
[3]*Physics Department, University of California, Riverside, California 92521, USA*

(Received 30 January 2021; accepted 25 March 2021; published 30 April 2021)

The associated production of a single-top with opposite-sign same-flavor (OSSF) dileptons, $pp \to t\ell^+\ell^-$ and $pp \to t\ell^+\ell^- + j$ ($j =$ light jet), can lead to striking trilepton $pp \to \ell'\ell^+\ell^- + X$ and dilepton $pp \to \ell^+\ell^- + j_b + X$ ($j_b = b$-jet) events at the LHC, after the top decays. Although these rather generic multilepton signals are flavor-blind, they can be generated by new 4-Fermi flavor changing (FC) $u_i t\ell\ell$ scalar, vector and tensor interactions ($u_i \in u, c$), which we study in this paper; we match the FC $u_i t\ell\ell$ 4-Fermi terms to the SMEFT operators and also to different types of FC underlying heavy physics. The main backgrounds to these di- and trilepton signals arise from $t\bar{t}$, $Z +$ jets and $VV$ ($V = W, Z$) production, but they can be essentially eliminated with a sufficiently high invariant mass selection on the OSSF dileptons, $m^{\rm min}_{\ell^+\ell^-}(\text{OSSF}) \gtrsim 1$ TeV; the use of $b$-tagging as an additional selection in the dilepton final state case also proves very useful. We find, for example, that the expected 95% CL bounds on the scale of a tensor(vector) $ut\mu\mu$ interaction, with the current $\sim 140\ \text{fb}^{-1}$ of LHC data, are $\Lambda \lesssim 5(3.2)$ TeV or $\Lambda \lesssim 4.1(2.7)$ TeV, if analyzed via the dimuon $\mu^+\mu^- + j_b$ signal or the $e\mu^+\mu^-$ trilepton one, respectively. The expected reach at the HL-LHC with 3000 $\text{fb}^{-1}$ of data is $\Lambda \lesssim 7.1(4.7)$ TeV and $\Lambda \lesssim 2.4(1.5)$ TeV for the corresponding $ut\mu\mu$ and $ct\mu\mu$ operators. This should be compared to the current bounds of $\Lambda \lesssim \mathcal{O}(1)$ TeV on both the $ut\ell\ell$ and $ct\ell\ell$ operators from LEP2 and from $pp \to t\bar{t}$ followed by $t \to \ell^+\ell^- j$. We also study the potential sensitivity at future 27 TeV and 100 TeV high-energy LHC successors, which, for the $ut\ell\ell$ operators, can reach $\Lambda \sim 10$–40 TeV. We furthermore discuss the possible implications of this class of FC 4-Fermi effective interactions on lepton nonuniversality tests at the LHC.

DOI: 10.1103/PhysRevD.103.075031

## I. INTRODUCTION

The origin of the observed flavor pattern in the fermion sector still remains one of the fundamental unresolved questions in theoretical particle physics. In particular, tree-level flavor-changing neutral currents (FCNC) are absent in the Standard Model (SM), so that FCNC effects in the SM are, in many cases, vanishingly small since they can only arise at the loop level and are GIM suppressed; this is the case for $t \to u$ and $t \to c$ transitions in top decays [1–10] and/or top-production processes [11–18]. Thus, the feeblest signal of FCNC effects in the top sector, either direct or indirect, may be an indicator of new flavor physics beyond the SM. This fact has led to a lot of theoretical as well as experimental activity in understanding and searching for top FCNC within model independent approaches, as well as within specific popular models beyond the SM.

The significantly larger mass of the top-quark compared to all other quarks, best manifests the SM flavor problem and makes it the most sensitive to several types of new physics (NP) and, in particular, to new flavor and *CP*-violation physics [19]. For example, FCNC effects in decays of a quark will be typically suppressed by some power of $m_q/\Lambda$, where $\Lambda$ is the scale of the underlying NP, so that the larger the quark mass, the more significant the FCNC effects. For this reason, searching for new FC dynamics in the top-sector was and is one of the major goals of past, current and future colliders. However, unfortunately, after more than a decade of collecting data and searching for NP in numerous processes at the 7, 8 and 13 TeV LHC, it is now clear that the scale of any natural

*yoavafik@campus.technion.ac.il
†shaouly@physics.technion.ac.il
‡adlersoni@gmail.com
§jose.wudka@ucr.edu

underlying heavy physics and, in particular, the scale of possible flavor violation in the 3rd generation fermion sector, lies above $\Lambda \sim 1$–2 TeV. Indeed, even for decays of the top-quark, where the expected suppression factor for the corresponding NP-generated FC partial width is $(m_t/\Lambda)^n$ (typically $n = 4$ for FCNC top decays), the search for new underlying FC physics is extremely difficult.

On the other hand, the corresponding suppression factor for the cross-sections of any NP-generated FC scattering processes involving the top-quark, will be typically proportional to some power of $v/\Lambda$ or $E_{\rm cm}/\Lambda$, where $E_{\rm cm}$ is the c.m. energy of the collider. In particular, as we show below, the FC $t \to u$ and $t \to c$ transitions can be very efficiently studied in scattering processes, in some selected single-top production processes, where the FCNC effects are enhanced and SM backgrounds dramatically suppressed, i.e., at high $E_{\rm cm}$, which is particularly useful from the experimental point of view.

Having emphasized the advantages of using scattering processes at the LHC as a testing ground for NP and, in particular, for searches of FC effects in top-quark systems, we now turn to a concrete illustration of these general statements. We will consider the following dilepton and trilepton signals with a pair of opposite-sign same-flavor (OSSF) leptons:

$$pp \to \ell' \ell^+ \ell^- + X, \tag{1}$$

$$pp \to \ell^+ \ell^- + j_b + X, \tag{2}$$

where a selection of a single $b$-tagged jet is used with the dilepton final state and, in general, $\ell, \ell' = e,\ \mu$ or $\tau$ and $\ell' = \ell$ and/or $\ell' \neq \ell$ can be considered in the trilepton case. These di- and trilepton signals are useful for generic NP searches and, as it turns out, although they are flavor-blind, they can also be very effectively used to search for FCNC physics in the top sector.

We study here the effects of higher dimensional effective 4-Fermi $tu_i\ell\ell$ FC interactions,[1] where $u_i$ stands for either a $u$ or a $c$-quark and $\ell$ can be either of the three SM charged leptons, $\ell = e,\ \mu,\ \tau$.[2] Specifically, we will show that the higher dimensional FC $tu_i\ell\ell$ operators are best studied via the following single-top + dilepton associated production channels with 0 and/or 1 accompanying light-jet $j$ ($t$ stands for either a top or antitop quark)[3,4]:

$$\begin{aligned} &(t\ell\ell)_0:\ pp \to \ell^+\ell^- + t, \\ &(t\ell\ell)_1:\ pp \to \ell^+\ell^- + t + j, \end{aligned} \tag{3}$$

that lead to the dilepton and trilepton signals in (1) and (2), after the top decays via $t \to bW$ and, in the trilepton case, followed by $W \to \ell' \nu_{\ell'}$. Also, only the case of lepton flavor diagonal $tu_i\ell\ell$ 4-Fermi contact terms will be studied, so that the dileptons $\ell\ell$ in (3) and therefore also in (1) and (2) are OSSF. Note, though, that similar effects are expected from the lepton flavor violating $tu_i\ell\ell'$ 4-Fermi interactions if the underlying scale of lepton flavor violation is also at the multi-TeV scale, see e.g., [43–45]. Indeed, the presence of two-three high-$p_T$ charged leptons allows to have an efficient trigger strategy on such final states that can be used to very effectively cut down the event rate of the background. As will be shown, the new FC 4-Fermi $tu_i\ell\ell$ interactions can be isolated from the SM background, as well as from other potential sources of NP that can affect these $t\ell\ell$ signals, by looking at the off-Z peak behavior of the OSSF dileptons in the $(t\ell\ell)_0 \to \ell^+\ell^- + j_b,\ \ell'\ell^+\ell^-$ and $(t\ell\ell)_1 \to \ell^+\ell^- + j_b,\ \ell'\ell^+\ell^-$ signals from (3).

Let us recall that, in the SM, single-top production at the LHC proceeds via several channels with different underlying leading topologies:

(i) The so-called s-channel and t-channel $W$-exchange processes: $u\bar{d} \to t\bar{b}$ and $qb \to q't$ $(q, q' = u,\ d)$, respectively.

(ii) Single top production in association with a gauge-boson, which are initiated by b-quarks in the proton: $bg \to tW$ and $bW \to tZ/\gamma$. In the four flavor scheme, where only light quarks and gluons are allowed in the initial state, these processes are responsible for $tV$ + jets production, e.g., $pp \to tZj + j_b$, where $j_b$ stands for a $b$-jet (see Fig. 1).

(iii) Single top-Higgs associated production: $bW \to th$, which in the four flavor setup yields $pp \to thj$ and $pp \to thW$.

All the single-top channels mentioned above with the exception of the $tW$ and $tWj$ final states are pure electroweak (EW) processes. It is for this reason that these channels, including possible EFT FC effects, have been

[1]Some of the $t \to u_i$ 4-Fermi operators that we consider below are especially interesting, since by gauge invariance (see further discussion below), they also contribute to $b \to s\ell^+\ell^-$ and $b \to c\ell^-\nu_\ell$ transitions and, therefore, to the anomalies observed in the ratios $R_{K^{(*)}}$ and $R_{D^{(*)}}$ in neutral and charged semileptonic B-decays [20–40] (for a recent review see [41]). If confirmed, these anomalies would favor a multi-TeV scale for lepton-flavor nonuniversal (LFNU) new physics not only in $B$ decays, but also in the $t \to u, c$ transitions studied in this paper.

[2]We note that final states involving the $\tau$ have, in general, a lower experimental detection efficiency and are, therefore, expected to be less effective for our study.

[3]An interesting example of single-top production that can potentially lead to the dilepton and trilepton signals in (1) and (2) was recently studied in [42]. They investigated the effects of FC $Z'_\mu t_R \gamma^\mu u_R$ and $Z'_\mu t_R \gamma^\mu c_R$ couplings on the process $pp \to tZ'$, which can lead to the $(t\ell\ell)_0$ signal in (3) if the $Z'$ also couples to a pair of SM leptons.

[4]We note that a large charge asymmetry is expected, e.g., in $pp \to \ell'^+\ell^+\ell^-$ versus $pp \to \ell'^-\ell^+\ell^-$, due to an asymmetric production of top versus antitop quarks in (3) via $ug$-fusion (see Fig. 2), which is caused by the asymmetric $u$ versus anti-$u$ quark densities in the LHC $pp$ initial state.

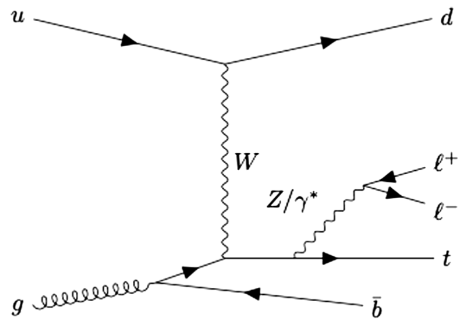


FIG. 1. Representative lowest-order Feynman diagrams for the SM single top-quark + dilepton production with one light jet, $pp \to t\ell^+\ell^- j$. Diagrams are shown for the on-Z peak (left) and non-resonant $\ell^+\ell^-$ (right) production cases.

widely studied in the past two decades [42,46–75]; a global and comprehensive analyses of the effects of various types of higher dimensional operators involving the top-quark field(s), including FC 4-Fermi operators of the type considered here (e.g., in [47]) can be found in [47–49, 52–56]. The effects of (2-quarks)(2-leptons) 4-Fermi operators (which are of interest in this study) on the single top + W production channel $pp \to tW \to \ell^+\ell^- + j_b + \not{E}_T$, had been recently studied in [76], where bounds at the level of $\Lambda \gtrsim$ few $\times$ 100 GeV were found on the scale of these operators. We note also the study in [77] of the effects of FC 4-quarks operators in single-top production via $q\bar{q} \to t + j$ ($j =$ light-quark jet).

Our $(t\ell\ell)_0$ zero-jets single-top + dilepton channel has, therefore, no significant, irreducible SM tree-level contribution: the process requires a FC $t \to u$ insertion, and the leading order SM diagrams for this process are 1-loop and are GIM suppressed. The combination of these effects renders the corresponding amplitude unobservably small within the SM. On the other hand, the $(t\ell\ell)_1$ channel $pp \to t\ell^+\ell^- j$ does have potentially significant SM contributions [78–82], which is dominated by the EW associated production of a single-top with a $Z$-boson and an accompanying light-jet, i.e., via $ub \to tZj$ in the five-flavor scheme, followed by the decay $Z \to \ell^+\ell^-$ as shown in the left diagram of Fig. 1. There is also a nonresonant contribution to $(t\ell\ell)_1$ (also depicted in Fig. 1) which is, however, subleading in the SM, consisting of no more than ~15% of the total cross section [79]. The process $(t\ell\ell)_1$ has been measured by both ATLAS [83,84] and CMS [85,86] collaborations, who focused on the on-$Z$ peak events, using a selection of $|m_{\ell^+\ell^-} - m_Z| < 10$ GeV for the signal region. The total (full phase-space) cross section was obtained by an extrapolation using the efficiency and acceptance factors calculated for the SM kinematics. In a very recent search by CMS [87], the effects of 4-Fermi $t\bar{t}\ell^+\ell^-$ operators (rather than the FC $tu_i\ell^+\ell^-$ operators relevant to our study) on the $(t\ell\ell)_1$ process and other top(s) + dilepton signals were studied (e.g., in $pp \to t\bar{t}\ell^+\ell^-$), where off-Z peak dilepton events were also considered with a selection $|m_{\ell^+\ell^-} - m_Z| > 10$ GeV, though they did not make use of the "hard" selection $m_{\ell^+\ell^-}(\text{OSSF}) >$ 1000 GeV that we utilize in this work.

Indeed, our main interest in this paper will be the potential NP effects that contribute to the OSSF cross section in the region of high dilepton invariant masses, e.g., $m_{\ell^+\ell^-}(\text{OSSF}) \gtrsim (100\text{–}1500)$ GeV. This will be the case, in particular, for the EFT contributions we study below. As we show below, large deviations from the SM are expected also off the Z-peak in the $(t\ell\ell)_0$ and $(t\ell\ell)_1$ single-top + dilepton channels of (3), in the presence of new top-quark couplings to leptons, which do not necessarily involve anomalous couplings of the SM gauge-bosons to the top-quark.

## II. NEW PHYSICS SETUP AND SINGLE-TOP + DILEPTON PRODUCTION AT THE LHC

The NP will be parametrized by higher dimensional, gauge-invariant effective operators, $\mathcal{O}_i^{(n)}$, in the so-called SM effective field theory (SMEFT) framework [88–92]; the effective operators are constructed using the SM fields and their coefficients are suppressed by inverse powers of the NP scale $\Lambda$ [88–92]:

$$\mathcal{L} = \mathcal{L}_{\text{SM}} + \sum_{n=5}^{\infty} \frac{1}{\Lambda^{n-4}} \sum_i \alpha_i O_i^{(n)}, \tag{4}$$

where $n$ is the mass dimension of $O_i^{(n)}$ and we assume decoupling and weakly-coupled heavy NP, so that $n$ equals the canonical dimension. The dominating NP effects are then expected to be generated by contributing operators with the lowest dimension (smallest $n$) that can be generated at tree-level in the underlying theory. The (Wilson) coefficients $\alpha_i$ depend on the details of the underlying heavy theory and, therefore, they parameterize all possible weakly-interacting and decoupling types of heavy physics; an example of matching this EFT setup to a specific underlying heavy NP scenario will be given below.

The dimension six operators ($n = 6$) include seven 4-Fermi operators, listed in Table I, that involve $t$ and $u$

TABLE I. The dimension six operators in the SMEFT, which potentially involve FC ($t \to u$) interactions between top-quarks and leptons and may, therefore, be a source for lepton nonuniversal effects (see also text). The subscripts $p$, $r$, $s$, $t$ are flavor indices.

| | |
|---|---|
| 4 − Fermi: $(\bar{L}L)(\bar{L}L)$ | |
| $\mathcal{O}_{lq}^{(1)}(prst)$ | $(\bar{l}_p\gamma_\mu l_r)(\bar{q}_s\gamma^\mu q_t)$ |
| $\mathcal{O}_{lq}^{(3)}(prst)$ | $(\bar{l}_p\gamma_\mu\tau^I l_r)(\bar{q}_s\gamma^\mu\tau^I q_t)$ |
| 4 − Fermi: $(\bar{R}R)(\bar{R}R)$ | |
| $\mathcal{O}_{eu}(prst)$ | $(\bar{e}_p\gamma_\mu e_r)(\bar{u}_s\gamma^\mu u_t)$ |
| 4 − Fermi: $(\bar{L}L)(\bar{R}R)$ | |
| $\mathcal{O}_{lu}(prst)$ | $(\bar{l}_p\gamma_\mu l_r)(\bar{u}_s\gamma^\mu u_t)$ |
| $\mathcal{O}_{qe}(prst)$ | $(\bar{e}_p\gamma^\mu e_r)(\bar{q}_s\gamma_\mu q_t)$ |
| 4 − Fermi: $(\bar{L}R)(\bar{L}R)$ + H.c.. | |
| $\mathcal{O}_{lequ}^{(1)}(prst)$ | $(\bar{l}_p^j e_r)\epsilon_{jk}(\bar{q}_s^k u_t)$ |
| $\mathcal{O}_{lequ}^{(3)}(prst)$ | $(\bar{l}_p^j\sigma_{\mu\nu} e_r)\epsilon_{jk}(\bar{q}_s^k\sigma^{\mu\nu} u_t)$ |

quarks and a pair of charged leptons and are relevant for the processes we consider. As will be discussed below, these operators may also generate LFNU effects. In Fig. 2 we depict representative diagrams for the $(t\ell\ell)_0$ and $(t\ell\ell)_1$ processes in (3), which are mediated by the $t\bar{u}\ell^+\ell^-$ 4-Fermi operators in Table I.

We will henceforward adopt the parametrization used in [93] for the effective Lagrangian of the FC $t\bar{u}\ell^+\ell^-$ contact interactions (a similar parametrization for the $t\bar{t}\ell^+\ell^-$ interactions has been used in [94,95] for the study of $e^+e^- \to t\bar{t}$), which was also used by the DELPHI [96] and L3 [97] collaborations at LEP2 to set bounds on the $tcee$ contact interactions resulting from the 4-Fermi operators of Table I (see also discussion below):

$$\mathcal{L}_{tu\ell\ell} = \frac{1}{\Lambda^2}\sum_{i,j=L,R}[V_{ij}^\ell(\bar{\ell}\gamma_\mu P_i\ell)(\bar{t}\gamma^\mu P_j u) + S_{ij}^\ell(\bar{\ell}P_i\ell)(\bar{t}P_j u) + T_{ij}^\ell(\bar{\ell}\sigma_{\mu\nu}P_i\ell)(\bar{t}\sigma_{\mu\nu}P_j u)], \tag{5}$$

where $P_{L,R} = (1 \mp \gamma_5)/2$ and $u$ represents a 1st or 2nd generation up-quark. In terms of the coefficients of the effective operators in Table I, the vectorlike ($V_{ij}^\ell$), scalarlike ($S_{ij}^\ell$), and tensorlike ($T_{ij}^\ell$) couplings are given by (we henceforward drop the superscript $\ell$):

$$\begin{aligned}
&V_{LL} = \alpha_{\ell q}^{(1)} - \alpha_{\ell q}^{(3)}, \qquad V_{LR} = \alpha_{\ell u},\\
&V_{RR} = \alpha_{eu}, \qquad V_{RL} = \alpha_{qe},\\
&S_{RR} = -\alpha_{\ell equ}^{(1)}, \qquad S_{LL} = S_{LR} = S_{RL} = 0,\\
&T_{RR} = -\alpha_{\ell equ}^{(3)}, \qquad T_{LL} = T_{LR} = T_{RL} = 0.
\end{aligned} \tag{6}$$

These 4-Fermi interactions can be generated through tree-level exchanges of heavy vectors and scalars in the underlying heavy theory (or their Fierz transforms). Note that no $LL$ tensor or $LL$, $LR$ and $RL$ scalar terms are generated at dimension 6; they can, however, be generated by dimension 8 operators and thus have coefficients suppressed by $\sim(v^2/\Lambda^4)$, where $v = 246$ GeV is the Higgs vacuum expectation value.

### A. Examples of matching to underlying beyond the SM scenarios

Interesting examples of underlying heavy particle tree-level exchanges that can generate some of the $tu_i\ell\ell$ operators above include the $R_2$-type scalar leptoquark (this is the only scalar leptoquark that does not induce proton decay) and the $U_1$-type vector leptoquark, which transforms as $(3, 2, 7/6)$ and $(3, 1, 2/3)$ under the $SU(3) \times SU(2) \times U(1)$ SM gauge group, respectively. These two leptoquarks can address both $R_{K^{(*)}}$ and $R_{D^{(*)}}$ anomalies as well as the muon $g-2$ one (see [98–105] for the $R_2$ case and [106–111] for the $U_1$ case), having the following couplings to a quark-lepton pair [112]:

$$\mathcal{L}_Y^{R_2} = z\bar{e}R_2^{i\star}q^i - y\bar{u}R_2^i\epsilon_{ij}\ell^j + \text{H.c.}, \tag{7}$$

$$\mathcal{L}_Y^{U_1} \supset x\bar{q}\gamma_\mu U_1^\mu\ell + \text{H.c.}, \tag{8}$$

where $i$, $j$ are $SU(2)$ indices and flavor indices are not specified ($U_1$ can have additional $d_R\gamma_\mu e_R$ and $u_R\gamma_\mu\nu_R$

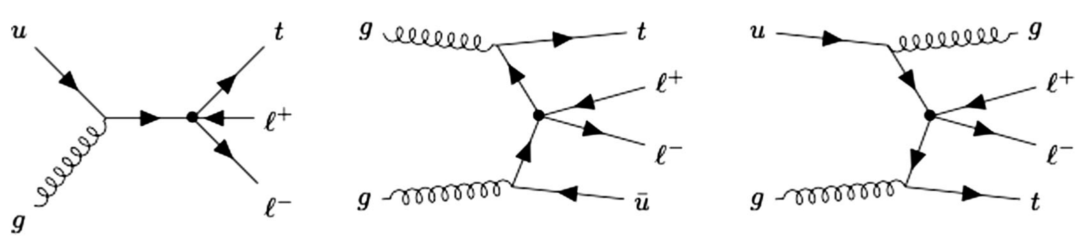


FIG. 2. Representative Feynman diagrams for the lowest order single top-quark + dilepton production channels with no light jets $pp \to t\ell^+\ell^-$ (left) and with one light jet $pp \to t\ell^+\ell^- + j$ (middle and right) at the LHC, via the $t\bar{u}\ell^+\ell^-$ 4-Fermi interaction (marked by a heavy dot).

couplings which are not relevant to our setup). In particular, tree-level exchanges of $R_2$ and $U_1$ among the lepton-quark pairs induce (after a Fierz transformation) [105,113]:

$$\begin{aligned} U_1\colon\ \alpha^{(1)}_{\ell q} &= \alpha^{(3)}_{\ell q} = -\frac{xx^\star}{2M^2_{U_1}}, \\ R_2\colon\ \alpha_{qe} &= -\frac{zz^\star}{2M^2_{R_2}}, \qquad \alpha_{\ell u} = \frac{yy^\star}{2M^2_{R_2}}, \\ \alpha^{(1)}_{\ell equ} &= 4\alpha^{(3)}_{\ell equ} = -\frac{yz}{2M^2_{R_2}}, \end{aligned} \tag{9}$$

where $M_{R_2}$ and $M_{U_1}$ are the masses of $R_2$ and $U_1$, respectively. Thus, following our parametrization in Eq. (5), we see that the 4-Fermi vector couplings $V_{RL}$ and $V_{LR}$ as well as the scalar and tensor couplings $S_{RR}$ and $T_{RR}$ can be generated in the underlying heavy theory if it includes the leptoquarks $R_2$, and if this leptoquark couples, e.g., to top-muon and up-muon (or charm-muon) pairs. It is interesting to note that, although $U_1$ contributes to the operators $\mathcal{O}^{(1)}_{\ell q}$ and $\mathcal{O}^{(3)}_{\ell q}$, it does not generate the $V_{LL}$ vector interactions of (5), since $\alpha^{(1)}_{\ell q} = \alpha^{(3)}_{\ell q}$ if $\mathcal{O}^{(1)}_{\ell q}$ and $\mathcal{O}^{(3)}_{\ell q}$ are generated by $U_1$. On the other hand, it will generate the $V_{LL}$ terms for the corresponding down-quark operators, e.g., $(\bar{\ell}\gamma_\mu P_i \ell)(\bar{b}\gamma^\mu P_j s)$, for which $V_{LL} = \alpha^{(1)}_{\ell q} + \alpha^{(3)}_{\ell q}$, see e.g., [113].

A compilation of the various types of NP that can induce the dimension six 4-Fermi interactions in Table I can be found in [44].

## III. BOUNDS AND RELATED PHENOMENOLOGY

We now briefly summarize the current bounds and phenomenology aspects related to the $tu_i\ell\ell$ 4-Fermi contact interactions of Eq. (5).

### A. The $tu_iee$ 4-Fermi operators involving two electrons

These operators can contribute to single top-quark + light-jet production at an $e^+e^-$ machine: $e^+e^- \to t + j$, where the light-jet $j$ originates from either a $u$ or a $c$-quark. Accordingly, these operators were studied and constrained at LEP2 by the DELPHI [96] and L3 [97] collaborations, who reported bounds ranging from $\Lambda \gtrsim 600$ GeV to $\Lambda \gtrsim 1.4$ TeV, depending on the underlying NP mechanism, i.e., whether a scalar, vector or tensor-like $tu_iee$ 4-Fermi vertex is involved, and assuming $\mathcal{O}(1)$ couplings for these interactions. A slight improvement can be obtained by combining these LEP2 bounds with (the rather weak) bounds derived from the rare top decay to a pair of charged leptons and a jet $t \to \ell^+\ell^- j$ [43,44,47,77,114].[5]

[5] The partial FC top decay width $\Gamma_{\ell\ell u} = \Gamma(t \to \ell^+\ell^- u)$ due to the 4-Fermi $tu_i\ell\ell$ scalar, vector and tensor interactions of (5) is: $\Gamma_{\ell\ell u} = (2\pi m_t/3)[m_t/(8\pi\Lambda)]^4 \cdot (S^2_{RR} + 4\sum V^2_{ij} + 48 T^2_{RR})$ [44,77].

### B. The $tu_i\mu\mu$ 4-Fermi operators involving two muons

The constraints on these operators are weak due to the absence of experimental bounds off the Z peak. In particular, bounds on these operators can be derived from $pp \to t\bar{t}$ production at the LHC, followed by $t \to \ell^+\ell^- j$ by one of the top-quarks, but no off-Z peak data was analyzed in this channel. Note, however, the recent interesting analysis performed in [44] extending existing $t \to Zj$ experimental searches in $t\bar{t}$ production at the LHC, using an off-Z peak dilepton invariant mass selection to put new bounds on the scale of $tu_i\ell\ell$ 4-Fermi operators of Table I. They found e.g., that $\Lambda \gtrsim 0.8, 1.0, 1.5$ TeV can be reached at the future HL-LHC on the scalar, vector and tensor $tu\mu\mu$ and $tc\mu\mu$ interactions, respectively, for $\mathcal{O}(1)$ couplings: $S_{RR} = V_{ij} = T_{RR} = 1$. These bounds are comparable to the LEP2 bounds on $tuee$ and $tcee$ discussed above, but, as we will show below, fall short by a factor of 3-5 compared to the sensitivity that can be obtained using the single-top + dilepton channels considered in this work.

### C. Implications of gauge invariance: Consequences for $b$-quark scattering and $B$-physics

In operators involving left-handed quark isodoublets gauge invariance relates the $tu\ell\ell$ and $bd\ell\ell$ 4-Fermi FC interactions.[6] In particular, among the operators in Table I, the $(\bar{L}L)(\bar{L}L)$ operators $\mathcal{O}^{(1)}_{lq}$, $\mathcal{O}^{(3)}_{lq}$ and the $(\bar{L}R)(\bar{R}L)$ one $\mathcal{O}_{qe}$, include also the corresponding FCNC $bd\ell\ell$ interactions:

$$\begin{aligned} \mathcal{O}^{(1)}_{lq}(pr31) &= (\bar{\ell}_p\gamma_\mu P_L \ell_r)\cdot[(\bar{t}\gamma^\mu P_L u) + (\bar{b}\gamma^\mu P_L d)], \\ \mathcal{O}^{(3)}_{lq}(pr31) &\supset (\bar{\ell}_p\gamma_\mu \tau^3 P_L \ell_r)\cdot[(\bar{t}\gamma^\mu P_L u) - (\bar{b}\gamma^\mu P_L d)], \\ \mathcal{O}_{qe}(pr31) &= (\bar{\ell}_p\gamma^\mu P_R \ell_r)\cdot[(\bar{t}\gamma_\mu P_L u) + (\bar{b}\gamma_\mu P_L d)]. \end{aligned} \tag{10}$$

Referring to (5) it then follows that the $V_{LL}$ and $V_{RL}$ couplings for the $t$ and $b$ quarks are related: $V_{LL}(tu\ell\ell) = \alpha^{(1)}_{\ell q} - \alpha^{(3)}_{\ell q}$, $V_{LL}(bd\ell\ell) = -\alpha^{(1)}_{\ell q} - \alpha^{(3)}_{\ell q}$ and $V_{RL}(tu\ell\ell) = V_{RL}(bd\ell\ell) = \alpha_{qe}$, and the corresponding scales $\Lambda$ are the same. Similar relations occur for operators involving left-handed quarks of the 2nd and 3rd generations, e.g., $V_{RL}(tc\ell\ell) = V_{RL}(bs\ell\ell)$.

The triplet operator $\mathcal{O}^{(3)}_{lq}(pr31)$ also includes the 4-Fermi charged currents, e.g., for the muon case: $(t\gamma_\mu P_L d)(\mu\gamma^\mu P_L \nu_\mu)$ and $(b\gamma_\mu P_L u)(\mu\gamma^\mu P_L \nu_\mu)$, and, similarly, $\mathcal{O}^{(3)}_{lq}(pr32) \supset (t\gamma_\mu P_L s)(\mu\gamma^\mu P_L \nu_\mu)$, $(b\gamma_\mu P_L c)(\mu\gamma^\mu P_L \nu_\mu)$. Furthermore, the $(\bar{L}R)(\bar{L}R)$ scalar and tensor operators

[6] Note that the correlation between operators involving the top-quark and operators involving the $b$-quark should be taken with caution, since sign differences can lead to e.g., a cancellation of effects for operators involving $b_L$ and an enhancement for those involving $t_L$ (or vice-versa).

$\mathcal{O}^{(1)}_{lequ}(pr31)$ and $\mathcal{O}^{(3)}_{lequ}(pr31)$ induce the charged currents involving the $b$-quark: $(\bar{b}P_R u)(\bar{\nu}_\mu P_R \mu)$, $(\bar{b}\sigma^{\mu\nu}P_R u)(\bar{\nu}_\mu \sigma_{\mu\nu} P_R \mu)$ and similarly the $b \to c$ ones for $\mathcal{O}^{(1)}_{lequ}(pr32)$ and $\mathcal{O}^{(3)}_{lequ}(pr32)$.

Therefore, the $V_{LL}$, $V_{RL}$, $S_{RR}$ and $T_{RR}$ 4-Fermi $tu\ell\ell$ and $tc\ell\ell$ terms in (5), have also interesting repercussions in scattering processes involving the b-quark in the final state, e.g., $dg \to b\ell\ell$ [115–119], in $bq$ scattering e.g., $bd \to \ell\ell$, $bu \to \ell\nu_\ell$ [120–122] as well as in B-decays (see e.g., [107,123]). For the latter, some of the notable ones include $B^+ \to \pi^+\mu^+\mu^-$, $B^+ \to K^+\mu^+\mu^-$ and $B^0_{d,s} \to \mu^+\mu^-$ associated with $b \to d$ transitions, see e.g., the recent analysis in [113], as well as the $R_{K^{(*)}}$ and $R_{D^{(*)}}$ anomalies [20–41], which occur in $b \to s\ell^+\ell^-$ and $b \to c\ell^-\nu_\ell$ transitions, respectively, and may, therefore, be closely related to the $tu_i\ell\ell$ dynamics discussed in this work (see also [124–126]). In particular, a best fit to $R_{K^{(*)}}$, $R_K$ and $B^0_s \to \mu^+\mu^-$ observables implies that the scale of $\mathcal{O}^{(1)}_{lq}(pr32)$ or $\mathcal{O}^{(3)}_{lq}(pr32)$ (or both) is around 40 TeV [113] assuming no cancellations, in which case the contribution of these operators to our single-top production processes is too small to be observed at the 13 TeV LHC. Alternatively, if single top production effects involving $\mathcal{O}^{(1,3)}_{lq}$ are observed at the LHC, this would indicate not only the presence of NP, but also that cancellations do in fact occur ($\alpha^{(1)}_{lq} \simeq \alpha^{(3)}_{lq}$), giving additional information about the properties of the new physics involved.

### D. Implications of gauge invariance: $pp \to t + \not{E}_T$ and $pp \to t\ell + \not{E}_T$ single-top signals

The $(\bar{L}L)(\bar{L}L)$ vector operator $\mathcal{O}^{(3)}_{lq}$ as well as the $(\bar{L}R)(\bar{L}R)$ scalar and tensor 4-Fermi operators $\mathcal{O}^{(1)}_{lequ}$ and $\mathcal{O}^{(3)}_{lequ}$, which contribute to the FCNC $tu_i\ell\ell$ interactions ($u_i \in u, c$), also include (by virtue of gauge invariance) the charged 4-Fermi currents $td\ell\nu_\ell$ ($d \in d, s$). As such, these operators will also lead to the single-top + single-lepton signals with 0 and 1 accompanying light jet and missing energy, in analogy to the dilepton signals of (3):

$$pp \to \ell + t + \not{E}_T$$
$$pp \to \ell + t + j + \not{E}_T, \tag{11}$$

where the underlying production mechanisms for these processes are similar to the ones depicted in Fig. 2, replacing $u \to d$ and one of the charged leptons with a neutrino in these diagrams.[7]

[7]Note that another related operator $\mathcal{O}_{ledq} = (\bar{\ell}e)(\bar{d}q)$, which is not considered in this work (i.e., since it does not yield the FC $tu_i\ell\ell$ interactions that lead to our single-top + dilepton signals) can also contribute to the mono-top + single-lepton signals in (11).

TABLE II. Processes affected by the six 4-Fermi $tu_i\ell\ell$ operators type, due to gauge invariance. $b/B$-physics stands for scattering processes, not involving top-quarks, with b-quark either in the initial or the final state, and/or NP in $B$-decays. See also text.

| | $tu_i\ell\ell$ 4-Fermi type | | | | | |
|---|---|---|---|---|---|---|
| signal | $S_{RR}$ | $T_{RR}$ | $V_{RR}$ | $V_{LL}$ | $V_{RL}$ | $V_{LR}$ |
| $pp \to t\ell\ell/t\ell\ell + j$ | ✓ | ✓ | ✓ | ✓ | ✓ | ✓ |
| $pp \to t\ell + \not{E}_T/t\ell + j + \not{E}_T$ | ✓ | ✓ | | ✓ | | |
| $pp \to t + \not{E}_T/t + j + \not{E}_T$ | | | | ✓ | | ✓ |
| $b/B$-physics | ✓ | ✓ | | ✓ | ✓ | |

Similarly, the $(\bar{L}L)(\bar{L}L)$ operators $\mathcal{O}^{(1)}_{lq}$, $\mathcal{O}^{(3)}_{lq}$ and the $(\bar{L}L)(\bar{R}R)$ operator $\mathcal{O}_{lu}$ with flavor indices contributing to the $tu_i\ell\ell$ interactions, also generate (again, by virtue of gauge invariance) the FCNC 4-Fermi terms involving only neutrinos, i.e., $tu_i\nu_\ell\nu_\ell$. They therefore also lead to the following signals of a single-top $+ \not{E}_T$ with and without a light-jet (and without charged leptons):

$$pp \to t + \not{E}_T$$
$$pp \to t + j + \not{E}_T, \tag{12}$$

where, here also, the underlying diagrams for these processes are similar to the ones depicted in Fig. 2, replacing the two charged leptons with two neutrinos.

These single-top + single (charged) lepton $+ \not{E}_T$ and single-top $+ \not{E}_T$ signals are more challenging, since they are expected to have a significantly larger SM background, e.g., from $t\bar{t}$ production. Nonetheless, a dedicated study of such beyond the SM signals is called for, where the correlations between the no-lepton, monolepton, and dilepton single-top signals can be exploited to gain a better sensitivity, as we have recently demonstrated in [119].

Following the above discussion, in Table II we draw a chart which maps the contributions of the six types of 4-Fermi $tu_i\ell\ell$ operators studied here to the different types of single-top production processes and to $b/B$-physics. We see that $V_{RR}$ is the only operator which affects only the single-top + dilepton signals studied in this work, without influencing the other single-top channels and $b/B$-physics.

## IV. SIGNAL AND BACKGROUND ANALYSIS

In this section we will describe the essential ingredients for the signal over background analysis of the single top + dilepton signal. Specifically, we will provide a sensitivity study to the NP signals, based on simplified criteria. A more realistic analysis will be presented in the next section.

We will use an $m_{\ell\ell}$-dependent integrated cross section, selecting events above a minimum value of $m_{\ell\ell}$:

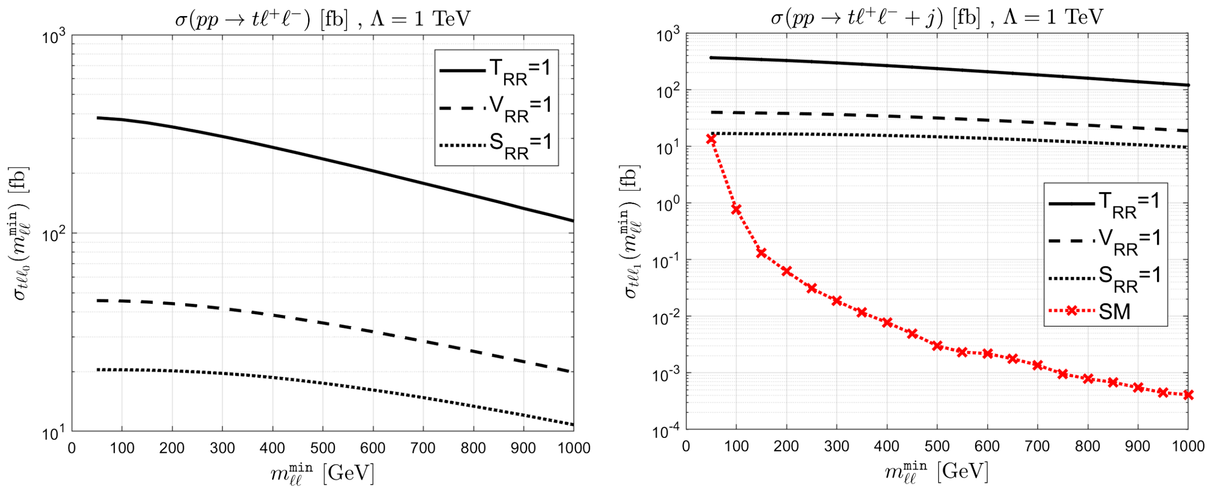


FIG. 3. Integrated cross sections for the $(t\ell\ell)_0$ and $(t\ell\ell)_1$ single-top + dilepton channels, as a function of the lower dilepton invariant mass cut, see (14). The NP effects are calculated with $\Lambda = 1$ TeV and $f = 1$, where $f = V_{RR}$, $f = S_{RR}$ or $f = T_{RR}$.

$$\sigma(m_{\ell\ell}^{\min}) \equiv \sigma(m_{\ell\ell} \geq m_{\ell\ell}^{\min}) = \int_{m_{\ell\ell} \geq m_{\ell\ell}^{\min}} dm_{\ell\ell} \frac{d\sigma}{dm_{\ell\ell}}, \quad (13)$$

where $m_{\ell\ell}^{\min}$ will be chosen to optimize the analysis sensitivity. In the next section we will also impose an upper cut, $m_{\ell\ell} \leq m_{\ell\ell}^{\max}$, that will be used to ensure the applicability of the EFT approach we adopt.

The cross section for the single-top + dilepton production channels in (3) can then be written in the general form

$$\sigma_{t\ell\ell_j}(m_{\ell\ell}^{\min}) = \sigma_{t\ell\ell_j}^{\mathrm{SM}}(m_{\ell\ell}^{\min}) + \frac{f^2}{(\Lambda/[\mathrm{TeV}])^4} \cdot \sigma_{t\ell\ell_j}^{\mathrm{NP}}(m_{\ell\ell}^{\min}), \quad (14)$$

where $\sigma_{t\ell\ell_j}^{\mathrm{SM}}(m_{\ell\ell}^{\min})$ and $\sigma_{t\ell\ell_j}^{\mathrm{NP}}(m_{\ell\ell}^{\min})$ are the $m_{\ell\ell}$-dependent SM and NP[2] integrated cross sections, respectively. We recall that $\sigma_{t\ell\ell_0}^{\mathrm{SM}} = 0$ at tree-level and that the 1-loop contribution is vanishingly small (see the discussion in Sec. I). Furthermore, the NP diagrams are QCD-generated (via gluon-quark and gluon-gluon fusion, see Fig. 2) and, in the $t\ell\ell_1$ case, they do not interfere with the SM, which is electroweak-generated and involves a different final state (see Fig. 1). Therefore, there is no term $\propto 1/\Lambda^2$ for both the $t\ell\ell_0$ and $t\ell\ell_1$ channels, so that the leading NP terms are scaled by the NP couplings $f^2/\Lambda^4$, where $f$ is the dimensionless coefficient of the 4-Fermi $tu_i\ell\ell$ interactions in (5) and (6), i.e., $f = V_{ij}, S_{ij}$ or $T_{ij}$ for the vector, scalar, or tensorlike terms and we will take $f = 1$ henceforward for simplicity.

All cross sections reported in this section were calculated using MADGRAPH5_aMC@NLO [127] at LO parton-level and a dedicated universal FeynRules output (UFO) model for the EFT framework was produced using FeynRules [128]. We have used the LO MSTW 2008 parton distribution functions (PDF) set (MSTW2008lo68cl [129]) in the 5-flavor scheme with a dynamical scale choice for the central value of the factorization ($\mu_F$) and renormalization ($\mu_R$) scales, i.e., corresponding to the sum of the transverse mass in the hard-processes. As a baseline selection, we used: $p_T(j) > 35$ GeV, $|\eta(j)| < 4.5$ for jets and $p_T(\ell) > 25$ GeV,$|\eta(\ell)| < 2.5$ for leptons. Also, the minimum angular distance in the $\eta - \phi$ plane between all objects (leptons and jets) is $> 0.4$ and kinematic selections cuts (i.e., on the dilepton invariant mass) were imposed using MADANALYSIS5 [130].

To get an estimate of the sensitivity of the results to the lower cut selection of the dilepton invariant mass $m_{\ell\ell}^{\min}$, we plot in Fig. 3 and list in Table III the NP and SM integrated $t\ell\ell_j$ cross sections, as a function of $m_{\ell\ell}^{\min}$ (at this point without an upper cut selection $m_{\ell\ell}^{\max}$), where the NP terms were calculated for the scalar, vector, and tensor 4-Fermi operators with the benchmark values of $\Lambda = 1$ TeV and $f = 1$ ($f = S_{RR}, V_{RR}, T_{RR}$). Results for different choice of $\Lambda$ and/or $f$ are obtained by scaling the cross section by $f^2/\Lambda^4$. We see that selecting high $m_{\ell\ell}$ dilepton events, $m_{\ell\ell}^{\min} > 100$ GeV, the SM contribution for the $(t\ell\ell)_1$ is dramatically suppressed (i.e., by about five orders of magnitude in going from $m_{\ell\ell}^{\min} = 50$ GeV to $m_{\ell\ell}^{\min} = 1$ TeV). With this choice we have $\sigma_{t\ell\ell_1}^{\mathrm{SM}} \ll \sigma_{t\ell\ell_1}^{\mathrm{NP}}$, so that the SM contribution can also be ignored in (14). Indeed, as shown below, we obtain a better sensitivity to the NP with a higher $m_{\ell\ell}^{\min}$ selection, for which, not only the SM irreducible background effectively vanishes, but also the potential reducible SM background is essentially eliminated.

In the following we will study the sensitivity only to the $S_{RR}$, $V_{RR}$, and $T_{RR}$ 4-Fermi interactions, noting that, since we are mainly analysing total cross sections and since there are no SM × NP interference effects (see discussion above), the sensitivity and reach for the other

TABLE III. The integrated cross sections of the pure NP contributions to the processes $(t\ell\ell)_0$ and $(t\ell\ell)_1$ of (3), i.e., $\sigma^{\rm NP}_{t\ell\ell_0}$ and $\sigma^{\rm NP}_{t\ell\ell_1}$ in (14), and of the SM part in the $(t\ell\ell)_1$ channel, $\sigma^{\rm SM}_{t\ell\ell_1}$ in (14), for the dilepton invariant mass lower cut selections $m^{\rm min}_{\ell\ell} = 50$, 100, 300, 1000 GeV. The NP contributions are calculated with $\Lambda = 1$ TeV and $f = 1$, where $f = S_{RR}$, $T_{RR}$ or $f = V_{RR}$. See also text.

| Source | Integrated cross section [fb], $\Lambda = 1$ TeV | | | |
|---|---|---|---|---|
| | $m^{\rm min}_{\mu^+\mu^-} = 50$ GeV | $m^{\rm min}_{\mu^+\mu^-} = 100$ GeV | $m^{\rm min}_{\mu^+\mu^-} = 300$ GeV | $m^{\rm min}_{\mu^+\mu^-} = 1000$ GeV |
| NP: $pp \to t\ell^+\ell^-$ ($S_{RR} = 1$ | 20.5 | 20.4 | 19.6 | 10.8 |
| NP: $pp \to t\ell^+\ell^-$ ($T_{RR} = 1$ | 381.2 | 373.3 | 306.9 | 114.9 |
| NP: $pp \to t\ell^+\ell^-$ ($V_{RR} = 1$ | 45.6 | 45.5 | 41.6 | 19.8 |
| NP: $pp \to t\ell^+\ell^- j$ ($S_{RR} = 1$ | 16.8 | 16.7 | 16.1 | 9.6 |
| NP: $pp \to t\ell^+\ell^- j$ ($T_{RR} = 1$ | 365.0 | 353.2 | 295.4 | 119.6 |
| NP: $pp \to t\ell^+\ell^- j$ ($V_{RR} = 1$ | 39.7 | 39.2 | 36.3 | 18.7 |
| SM: $pp \to t\ell^+\ell^- j$ | 13.6 | 0.77 | 0.019 | 0.00041 |

4-Fermi vector currents, $V_{LL}$, $V_{RL}$, and $V_{LR}$ is identical to that of $V_{RR}$.

### A. Event selection: signal vs background

To study the sensitivity to the NP, we will isolate the signal using either an inclusive trilepton selection criteria or a dilepton signature with an additional selection of a single $b$-tagged jet:[8]

$$(\ell'\ell\ell):\ pp \to \ell'\ell^+\ell^- + X, \tag{15}$$

$$(\ell\ell 1b):\ pp \to \ell^+\ell^- + j_b + X, \tag{16}$$

so that in the trilepton case we select events where the top decays via $t \to bW \to b\ell'\nu_{\ell'}$ and demand exactly 3 (isolated) charged leptons in the final state, where, in general, $\ell, \ell' = e$, $\mu$ or $\tau$ and $\ell' = \ell$ and/or $\ell' \neq \ell$ can be considered. An additional selection of a single $b$-tagged jet with the trilepton signal, i.e., $(\ell'\ell\ell 1b)$: $pp \to \ell'\ell^+\ell^- + j_b + X$ may in some cases also improve the sensitivity to the scale of the $tu_i\ell\ell$ 4-Fermi operators; we will briefly comment on that in the next section. We note that the $(\ell'\ell\ell)$ trilepton selection was recently used by both ATLAS [83,84] and CMS [85,86] in the measurement of the SM $pp \to t\ell^+\ell^- j$ cross section (see also [66,72, 78,87]). In fact, these trilepton signatures (with or without a high-$p_T$ jet; either light-jet or a $b$-jet) are rich in phenomenology, as they can probe several types of other well motivated TeV-scale NP scenarios, e.g., electroweak pair production of charginos and neutralinos in supersymmetry [131] and the production of a heavy neutral Majorana-type lepton [132].

We find that the trilepton $(\ell'\ell\ell)$ or dilepton $(\ell\ell 1b)$ signal selections of (15) and (16) along with the selection of events with high $\ell^+\ell^-$ invariant mass are sufficient to reduce the potential SM background to the level that it can be neglected. Furthermore, selecting a single $b$-tagged jet is found to be crucial in the case of the dilepton signal for efficiently tagging the top-quark decay in the final state and isolating the signal from the background (see also [116,117,121], where a better sensitivity for NP effects in dilepton events was obtained with a single $b$-tagged jet selection in $pp \to \mu^+\mu^- + j_b$ and $pp \to \tau\nu_\tau + j_b$).

As a case study, for the rest of this section we will assume that the NP generates only the dimuon 4-Fermi interactions and focus below either on the $(e\mu\mu)$ trilepton channel $pp \to e^\pm\mu^+\mu^- + X$ or the $(\mu\mu 1b)$ signal $pp \to \mu^+\mu^- + j_b + X$. We note, though, that similar analyses can be performed for the trilepton case in the channels $e\mu\mu, \mu\mu\mu, \tau\mu\mu$ or, more generally, for the channels $e\ell\ell, \mu\ell\ell, \tau\ell\ell$ when the NP generates the $tu_i\ell\ell$ operators for any given lepton flavor. Tri-lepton final states with 3 identical leptons can be similarly analyzed with appropriate selections on any pair of OSSF leptons. However, both the dilepton and trilepton final states involving the $\tau$ are more challenging and are expected to have a decreased sensitivity due to the lower experimental detection efficiency for the $\tau$.

The leading potential background for the $t\mu\mu$ and $t\mu\mu j$ signals arise from the SM $t\bar{t}$ and $\mu^+\mu^-$ + jets (dubbed hereafter as $Z$ + jets) production channels:

(i) $t\bar{t}$: $pp \to t\bar{t}$, followed by leptonic top-quark decays to muons $t\bar{t} \to \mu^+\mu^- + 2j_b + \not{E}_T$
(ii) $Z$ + jets: $pp \to \mu^+\mu^-$ + jets

which pass the trilepton selection when a nonprompt or fake lepton originate from hadronic decays or from misidentified jets. Additional sources of background, which we find to be subleading (see Table VII in the next section), include the $VV$, $tW$, $t\bar{t}V$ and $t\bar{V}V$ production channels, where $V = W, Z, \gamma$. For example, for the $(e\mu\mu)$ trilepton signal these are:

(i) $WZ$: $pp \to W\mu^+\mu^-$, followed by $W \to e\nu_e$
(ii) $ZZ$: $pp \to Z\mu^+\mu^-$, followed by $Z \to e^+e^-$ (contributes in case one electron is not tracked)
(iii) $tW$: $pp \to tW$, followed e.g., by $tW \to \mu^\pm\mu^\mp + j_b + 2j + \not{E}_T$ (+ a nonprompt electron, see text)

[8]Although top reconstruction will not be considered here, it may be useful for further reducing the background, e.g., the $VV$ and $Z$ + jets backgrounds considered below.

TABLE IV. Number of $(e\mu\mu)$ signal events per 100 fb$^{-1}$ of integrated luminosity, expected from the irreducible SM process $pp \to t\mu^+\mu^- j$ and from the pure NP $tu\mu\mu$ and $tc\mu\mu$ contributions to the fully inclusive $pp \to e\mu\mu + X$ signal as defined in (15), with dimuon invariant mass lower cut selections of $m^{\rm min}_{\mu^+\mu^-} = 100$, 300, 500, 1000 GeV. The NP contributions are calculated with $\Lambda = 1$ TeV and $f = 1$, where $f = S_{RR}, T_{RR}$ or $f = V_{RR}$. Note that the number of inclusive NP events includes the contributions from both $pp \to t\mu^+\mu^-$ and $pp \to t\mu^+\mu^- j$, followed by $t \to be\nu_e$. See also text.

| Source | Coupling | Number of inclusive $pp \to e\mu^+\mu^- + X$ signal events/100 fb$^{-1}$, $\Lambda = 1$ TeV | | | |
|---|---|---|---|---|---|
| | | $m^{\rm min}_{\mu^+\mu^-} = 100$ GeV | $m^{\rm min}_{\mu^+\mu^-} = 300$ GeV | $m^{\rm min}_{\mu^+\mu^-} = 500$ GeV | $m^{\rm min}_{\mu^+\mu^-} = 1000$ GeV |
| $\boldsymbol{tu\mu\mu}$ 4-Fermi | $S_{RR} = 1$ | 399 | 382 | 342 | 215 |
| | $T_{RR} = 1$ | 7937 | 6568 | 5117 | 2539 |
| | $V_{RR} = 1$ | 916 | 841 | 716 | 409 |
| $\boldsymbol{tc\mu\mu}$ 4-Fermi | $S_{RR} = 1$ | 29 | 25 | 20 | 9 |
| | $T_{RR} = 1$ | 711 | 481 | 318 | 108 |
| | $V_{RR} = 1$ | 75 | 60 | 44 | 18 |
| $pp \to t\mu^+\mu^- j$ | SM irreducible | 8 | 0 | 0 | 0 |

(iv) $t\bar{t}W$: $pp \to t\bar{t}\mu^\pm\nu_\mu$, followed by the leptonic top decays $t\bar{t} \to e^\pm\mu^\mp + 2j_b + \not{E}_T$ $pp \to t\bar{t}e^\pm\nu_e$, followed by $t\bar{t} \to \mu^+\mu^- + 2j_b + \not{E}_T$
(v) $t\bar{t}Z$: $pp \to t\bar{t}\mu^+\mu^-$, followed by the top decays $t\bar{t} \to e^\pm + 2j_b + 2j + \not{E}_T$
(vi) $t\bar{W}Z$: $pp \to tWZ$, followed by $Z \to \mu^+\mu^-$ and $tW \to e^\pm + j_b + 2j + \not{E}_T$

In Table IV we list the number of inclusive trilepton $pp \to e\mu^+\mu^-$ events per 100 fb$^{-1}$ of integrated luminosity, with the selections $m^{\rm min}_{\mu^+\mu^-} = 100$, 300, 500, 1000 GeV, generated by the $tu\mu\mu$ and $tc\mu\mu$ 4-Fermi operators and from the irreducible SM process $pp \to t\mu^+\mu^- j$. Note that the corresponding number of $pp \to \mu^+\mu^- + j_b$ events are 9 times larger than the number of inclusive trilepton $e\mu^+\mu^-$ events listed in Table IV, since all top decay channels $t \to bW$ followed by both the leptonic and the hadronic $W$-decays are included in this case. As discussed above, the $m^{\rm min}_{\mu^+\mu^-}$ selection is very effective for reducing the background to both the $(\mu\mu 1b)$ and $(e\mu\mu)$ signals; see Table VI and VII in the next section, where we list the yields from various sources of backgrounds to the $(\mu\mu 1b)$ and $(e\mu\mu)$ signals for the selections $m^{\rm min}_{\mu^+\mu^-} = 500$, 1000, 1500, 2000 GeV. For example, the background to the inclusive $(e\mu\mu)$ trilepton signal becomes negligible with the selection of $m^{\rm min}_{\mu^+\mu^-} \sim 1000$ GeV. Thus, to get an estimate of the sensitivity to the new $tu_i\mu\mu$ 4-Fermi operators, we will consider in the rest of this section only the inclusive $e\mu\mu$ trilepton signal case with $m^{\rm min}_{\mu^+\mu^-} = 1000$ GeV and assume that it is background free in this regime. A more realistic analysis including both the trilepton and dilepton + $b$-jet selections will be presented in the next section.

### B. Domain of validity of the EFT setup

The basic assumption underlying the EFT approach is that none of the heavy particles can be directly produced in the processes being investigated. Assuming that $\Lambda$ represents the masses of these particles, this leads to the requirement $\Lambda^2 \gtrsim \hat{s}$, where $\sqrt{\hat{s}}$ is the center-of-mass energy of the hard process. Alternatively, it is required that the NP cross sections do not violate tree-level unitarity bounds, which leads to similar constraints (for the case at hand the FC $tu_i\ell\ell$ 4-Fermi operators generate a cross section that grows with energy $\sigma^{\rm NP}_{t\ell\ell_j} \propto \hat{s}$). These criteria, however, are not precise enough for our purposes for the following reasons:

(i) The 4-fermion operators we consider can be generated either by a $Z$-like heavy particle coupling to lepton and quark pairs (eg. $tu_i \to X \to \ell\ell$), or by a leptoquark coupling to quark-lepton pairs (e.g., $t\ell \to \mathrm{LQ} \to u_i\ell$). In the first case the EFT is applicable when $\Lambda > m^{\rm max}_{\ell\ell}$, and in the second case when $\Lambda > m^{\rm max}_{q\ell}$. If only one of these conditions is obeyed the EFT approach remains applicable, but only for the corresponding type of new physics; only when *both* are violated is the EFT approach unreliable. It is worth noting that $\Lambda > m^{\rm max}_{q\ell}$ is often much less restrictive.
(ii) The constraints we derive will be on the effective scale $\Lambda_{\rm eff} = \Lambda/\sqrt{f}$, whence the EFT applicability conditions become $\Lambda_{\rm eff} > m^{\rm max}_{q\ell,\ell\ell}/\sqrt{f}$. Thus, the EFT approach remains applicable even for situations where $\Lambda_{\rm eff}$ is of the same order, or even somewhat smaller[9] than $m^{\rm max}_{q\ell,\ell\ell}$. This corresponds to NP scenarios with $f > 1$ (while still remaining perturbative).

[9]Note for example that applying the naive EFT validity criteria, $s < \Lambda^2_{\rm eff}$, to the Fermi theory of weak interactions would give $s < (246\ \mathrm{GeV})^2$ if $f = 1$, but in reality $f \sim 0.3$ and therefore $s \lesssim (100\ \mathrm{GeV})^2$.

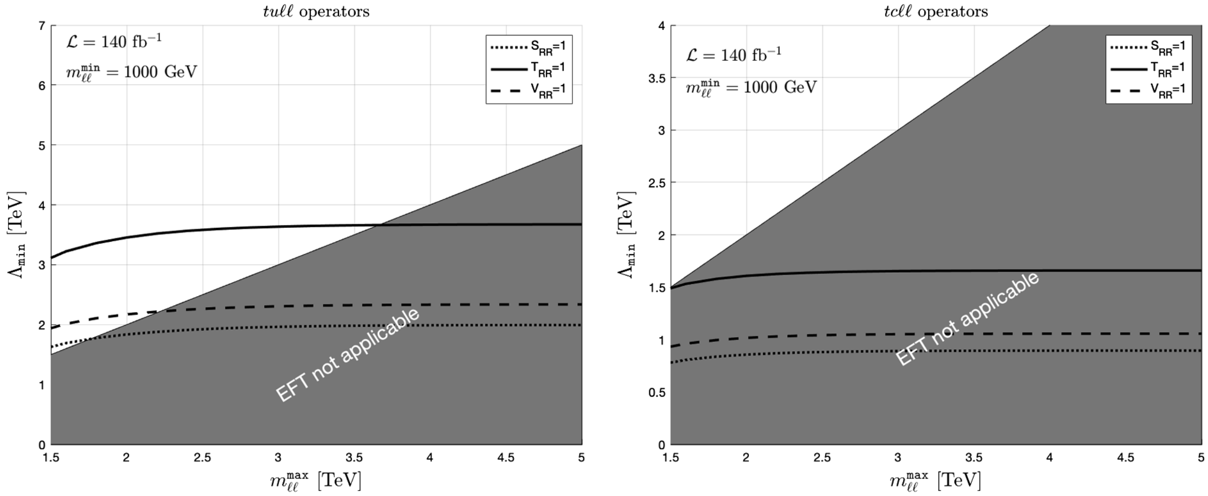


FIG. 4. Expected bounds ($\Lambda_{\rm min}$) on the scale $\Lambda$ (i.e., $\Lambda > \Lambda_{\rm min}$) from the trilepton signal $pp \to e\mu^+\mu^- + X$, for the scalar (dotted-line), vector (dashed-line) and tensor (solid-line) 4-Fermi $tu\mu\mu$ (left) and $tc\mu\mu$ (right) operators with $S_{RR} = 1$, $T_{RR} = 1$ and $V_{RR} = 1$, as a function of an upper cut on the dimuon invariant mass $m^{\rm max}_{\mu^+\mu^-}$. The bounds are calculated with $m^{\rm min}_{\mu^+\mu^-} = 1000$ GeV and for an integrated luminosity of $\mathcal{L} = 140\ {\rm fb}^{-1}$. The shaded areas correspond to the region where $m^{\rm max}_{\mu^+\mu^-} > \Lambda_{\rm min}$, which naively represents the domain outside the validity of the EFT prescription. See also text.

Based on this we will define the region of applicability by demanding $\Lambda > m^{\rm max}_{\ell\ell}$ *or* $\Lambda > m^{\rm max}_{q\ell}$, and allow $\Lambda_{\rm eff}$ to be smaller than $m^{\rm max}_{q\ell,\ell\ell}$ by an $O(1)$ factor.

To close this section we note that dimension 8 operators that interfere with the SM also generate $\mathcal{O}(\Lambda^{-4})$ contributions to the $pp \to t\mu^+\mu^- j$ cross section. These, however, can be ignored compared to the $\mathcal{O}(\Lambda^{-4})$ NP(dim .6) $\times$ NP(dim .6) terms that we keep, because the SM amplitude is much suppressed for the high $m^{\rm min}_{\ell\ell}$ selection that we use, as noted above.

### C. Sensitivity to the NP

We have not considered up to this point the theoretical and experimental uncertainties involved with the calculation and measurement of our $pp \to t\ell^+\ell^- + X \to \ell'\ell^+\ell^- + X$ signals. The theoretical uncertainties are due to the flavor scheme (i.e., 4-flavor vs 5-flavor), the NLO QCD (K-factor) and EW corrections, the dependence on the renormalization ($\mu_R$) and factorization ($\mu_F$) scales and the uncertainty due to the PDF choice. A detailed study of the SM dilepton + single-top associated production $pp \to t\ell^+\ell^- j$ was recently performed in [79], where it was found that these theory uncertainties amount to an $\mathcal{O}(10\%)$ uncertainty in the estimate of $\sigma(pp \to t\ell^+\ell^- j)$. It should be noted, though, that the uncertainties reported in [79] may not necessarily apply to out study, since our dominant signal processes are different (different initial and final states) and, also, we focus on a different kinematical region of the dilepton signals: the high dilepton invariant mass part of the phase-space, $m_{\ell^+\ell^-} > 1$ TeV (see below and in the next section).

Thus, the overall experimental uncertainty (i.e., statistical and systematic) for our inclusive trilepton signals is not known, in particular, in the high dilepton invariant mass regime (the sensitivity of our results to the overall uncertainty will be examine in the next section). Thus, to be on the conservative side, for an estimate of the sensitivity to the scale of the $tu_i\mu\mu$ 4-Fermi operators, we demand at least 20 inclusive $(e\mu\mu)$ trilepton events with the high $m^{\rm min}_{\mu\mu} = 1000$ GeV selection, which ensures at least 10 background-free NP events (see discussion above) even with an overall theoretical + experimental uncertainty of $\mathcal{O}(50\%)$. This condition corresponds to:

$$\frac{f^2}{(\Lambda/[{\rm TeV}])^4} \cdot \sigma^{\rm NP}_{e\mu\mu}(m^{\rm min}_{\mu\mu}) \cdot \mathcal{L} \geq 20, \tag{17}$$

where

$$\sigma^{\rm NP}_{e\mu\mu}(m^{\rm min}_{\mu\mu}) = [\sigma^{\rm NP}_{t\mu\mu_0}(m^{\rm min}_{\mu\mu}) + \sigma^{\rm NP}_{t\mu\mu_1}(m^{\rm min}_{\mu\mu})] \cdot {\rm BR}(t \to be\nu_e), \tag{18}$$

and $\sigma^{\rm NP}_{t\mu\mu_j}(m^{\rm min}_{\mu\mu})$ with $j = 0, 1$ are the NP parts of the integrated cross sections in (14) for the $(t\mu\mu)_0$ and $(t\mu\mu)_1$ single-top signals of (3).

The requirement (17) must be complemented with the constraints imposed by the validity of the EFT approach, $\Lambda > m^{\rm max}_{\ell\ell}$, as discussed in Sec. IV B above. As an example, we take $S_{RR} = V_{RR} = T_{RR} = 1$ (corresponding to $f = 1$ and $\Lambda = \Lambda_{\rm eff}$) and plot in Fig. 4 the expected bounds on $\Lambda$ ($\Lambda_{\rm min}$) of the scalar, vector and tensor $tu\mu\mu$ and $tc\mu\mu$ operators, as a function of the upper cut $m^{\rm max}_{\ell\ell}$, for

TABLE V. Expected bounds on the scale of the 4-Fermi $tu\mu\mu$ and $tc\mu\mu$ operators with $f = 1$ ($f = S_{RR}, T_{RR}, V_{RR}$) from the trilepton signal $pp \to e\mu^+\mu^- + X$ with a dimuon invariant mass lower cut selection of $m^{\rm min}_{\mu^+\mu^-} = 1000$ GeV and for integrated luminosities of $\mathcal{L} = 140$ and 3000 fb$^{-1}$. Entries marked with [EFT?] refer to cases where $\Lambda < m^{\rm max}_{\mu^+\mu^-}$, for which the applicability of the EFT approach is questionable. See also text.

| | | Expected bounds on $\Lambda$ [TeV], $m^{\rm min}_{\mu^+\mu^-} = 1000$ GeV | |
|---|---|---|---|
| | Coupling | ***tuμμ*** 4-Fermi case | ***tcμμ*** 4-Fermi case |
| $\mathcal{L} = 140$ fb$^{-1}$ | $S_{RR} = 1$ | 1.8 | 0.9 [EFT?] |
| | $T_{RR} = 1$ | 3.7 | 1.6 [EFT?] |
| | $V_{RR} = 1$ | 2.2 | 1.1 [EFT?] |
| $\mathcal{L} = 3000$ fb$^{-1}$ | $S_{RR} = 1$ | 4.3 | 1.8 |
| | $T_{RR} = 1$ | 7.9 | 3.6 |
| | $V_{RR} = 1$ | 5.0 | 2.2 |

an integrated luminosity of $\mathcal{L} = 140$ fb$^{-1}$ and a lower cut selection of $m^{\rm min}_{\mu^+\mu^-} = 1000$ GeV on the dimuon invariant mass. The shaded regions in Fig. 4 correspond to $m^{\rm max}_{\ell\ell} > \Lambda$, which as discussed above, is the domain where the validity of the EFT might be questionable. The corresponding bounds for integrated luminosities of $\mathcal{L} = 140$ and 3000 fb$^{-1}$ are summarized in Table V, where we note by [EFT?] the cases where the bound is not consistent with the (conservative) condition of $\Lambda > m^{\rm max}_{\ell\ell}$ on the applicability of the EFT approach, i.e., the cases where there is no crossing between the curves representing the bounds and the shaded area in Fig. 4.

We see, for example, that, with the current LHC data of about 140 fb$^{-1}$, no consistent bound can be derived on the scale of the $tc\ell\ell$ 4-Fermi operators using the criterion $\Lambda > m^{\rm max}_{\mu^+\mu^-}$ for $f = 1$, which restricts, but does not necessarily excludes, the EFT approach we adopted as discussed in Sec. IV B.

## V. A MORE REALISTIC STUDY

In order to have a more realistic prediction for the sensitivity to the $tu_i\mu\mu$ 4-Fermi NP terms, we have performed a more detailed analysis for the trilepton ($e\mu\mu$) and dilepton ($\mu\mu 1b$) signal selections of (15) and (16) with a pair of OSSF muons: $pp \to t\mu^+\mu^- + X \to e\mu^+\mu^- + X$ and $pp \to t\mu^+\mu^- + X \to \mu^+\mu^- + j_b + X$, where the electron and $b$-jet originate from the decay of the single-top in the final state.

### A. Simulated event samples

All event samples were again generated at LO using MADGRAPH5_aMC@NLO2.7.3 [127] in the 5-flavor scheme, using the dedicated UFO model mentioned earlier that was generated with FeynRules [128]. Here, the events were then interfaced with the PYTHIA8 [133] parton shower and we have used the NNPDF30LO PDF set [134] for samples at $\sqrt{s} = 13$ TeV and the PDF4LHC15 PDF set [135] for higher center-of-mass energies (27 and 100 TeV, see below). The default MADGRAPH5_aMC@NLO LO dynamical scale was used, which is the transverse mass calculated by a $k_T$-clustering of the final-state partons. Events of different jet-multiplicities were matched using the MLM scheme [136] using the default MADGRAPH5_aMC@NLO parameters and all samples were processed through DELPHES3 [137], which simulates the detector effects, applies simplified reconstruction algorithms and was used for the reconstruction of electrons, muons and hadronic jets. For the leptons (electrons and muons) the reconstruction was based on transverse momentum ($p_{\rm T}$)- and pseudorapidity ($\eta$)-dependent artificial efficiency weight and an isolation from other energy-flow objects was applied in a cone of $\Delta R = 0.4$ with a minimum $p_{\rm T}$ requirement of 30 GeV for each lepton. Jets were reconstructed using the anti-$k_t$ [138] clustering algorithm with radius parameter of $R = 0.4$ implemented in FastJet [139,140], and were required to have transverse momentum of $p_{\rm T} > 30$ GeV and pseudorapidity $|\eta| < 2.5$. In cases where a selection of a $b$-jet was used, the identification of $b$-tagged jets was done by applying a $p_{\rm T}$-dependent weight based on the jet's associated flavor, and the MV2c20 tagging algorithm [141] in the 70% working point.

Several types of background processes were considered (see also discussion in the previous section): (1) the production of 2-3 charged leptons through two gauge bosons (noted as $VV$); (2) the production of 2 muons via a neutral gauge boson (noted as $Z +$ jets); (3) the production of two muons from a decay of top-pair (noted as $t\bar{t}$) and (4) the production of two muons from the decays of top and $W$-boson produced via $pp \to tW$ (noted as $tW$). For the latter three, an additional non-prompt lepton, which originates e.g., from hadronic decays, can satisfy the trilepton selection criterion. Additional potential background processes (also mentioned earlier) from the SM processes $pp \to t\bar{t}W$, $t\bar{t}Z$, $tWZ$, $tZq$, were found to be negligible.

### B. Event selection

As noted above, our base-point selection contains two opposite-sign (OS) muons with an additional selection of either one electron in the trilepton $pp \to e\mu^+\mu^- + X$ case, or a single $b$-tagged jet for the dilepton signal $pp \to \mu^+\mu^- + j_b + X$. A requirement of an additional $b$-tagged jet with the trilepton signal, i.e., the selection ($e\mu\mu 1b$), will not be considered below, but we note that it can improve the sensitivity obtained with the ($e\mu\mu$) selection by about 10% in the high luminosity scenario of the HL-LHC.

The invariant mass of the OS muons ($m_{\mu^+\mu^-}$) was used for optimization in both cases, as the discriminating

TABLE VI. Number of reducible dilepton background events per 140 fb$^{-1}$ of integrated luminosity, expected from the SM processes $pp \to VV, t\bar{t}, Z + \text{jets}, tW \to \mu^+\mu^- + j_b + X$, with $m^{\min}_{\mu^+\mu^-} = 500, 1000, 1500, 2000$ GeV. See also text.

| | Number of background $pp \to \mu\mu + j_b + X$ events/140 fb$^{-1}$ | | | |
|---|---|---|---|---|
| Sub-process | $m^{\min}_{\mu^+\mu^-} = 500$ GeV | $m^{\min}_{\mu^+\mu^-} = 1000$ GeV | $m^{\min}_{\mu^+\mu^-} = 1500$ GeV | $m^{\min}_{\mu^+\mu^-} = 2000$ GeV |
| $VV$ | 13.0 | 1.2 | 0.2 | 0.1 |
| $t\bar{t}$ | 336.4 | 6.9 | 0.3 | 0.0 |
| $Z + \text{jets}$ | 128.2 | 10.9 | 1.9 | 0.4 |
| $Wt$ | 67.1 | 1.3 | 0.1 | 0.0 |
| Total $\mu\mu j_b$ Background events | 477.7 | 19.1 | 2.4 | 0.5 |

TABLE VII. Same as Table VI but for the case of the $(e\mu\mu)$ signal $pp \to e\mu^+\mu^- + X$.

| | Number of background $pp \to e\mu\mu + X$ events/140 fb$^{-1}$ | | | |
|---|---|---|---|---|
| Sub-process | $m^{\min}_{\mu^+\mu^-} = 500$ GeV | $m^{\min}_{\mu^+\mu^-} = 1000$ GeV | $m^{\min}_{\mu^+\mu^-} = 1500$ GeV | $m^{\min}_{\mu^+\mu^-} = 2000$ GeV |
| $VV$ | 7.1 | 1.0 | 0.2 | 0.1 |
| $t\bar{t}$ | 78.2 | 1.6 | 0.1 | 0.0 |
| $Z + \text{jets}$ | 16.5 | 1.3 | 0.2 | 0.0 |
| $Wt$ | 9.5 | 0.2 | 0.0 | 0.0 |
| Total $e\mu\mu$ Background events | 111.8 | 4.1 | 0.5 | 0.1 |

variable between the signal and the background; as shown in the previous section, the NP is expected to dominate at the tail of the $m_{\mu^+\mu^-}$ distribution whereas a small yield for the SM background is expected in that regime. We note that a dedicated selection for each signal scenario of the $tu\ell\ell$ or $tc\ell\ell$ operators can improve slightly the sensitivity, but, for simplicity, we keep the selection unified between all three signal scenarios (i.e., $S_{RR}$, $T_{RR}$, $V_{RR}$) of a given operator. Furthermore, as mentioned earlier, since the signal contains a single top-quark, a reconstruction of the top quark may also be useful for improving the sensitivity to the NP involved but we will not consider that here. Two values of the total integrated luminosity are considered below: 140 and 3000 fb$^{-1}$, which correspond to the currently available and HL-LHC integrated luminosities, respectively.

In Tables VI and VII we list the expected number of background events per 140 fb$^{-1}$ of integrated luminosity, for the dimuon + $b$-jet signal $pp \to \mu^+\mu^- + j_b + X$ and for the inclusive trilepton signal $pp \to e\mu^+\mu^- + X$, with dimuon invariant mass lower cut selections of $m^{\min}_{\mu^+\mu^-} =$ 500, 1000, 1500, 2000 GeV. In Fig. 5 we show the $m_{\mu^+\mu^-}$ distribution of the leading $VV$, $t\bar{t}$ and $Z + \text{jets}$ SM backgrounds and of the $(e\mu\mu)$ and $(\mu\mu 1b)$ signal scenarios for both the $tu\ell\ell$ and $tc\ell\ell V_{RR}$ operators.

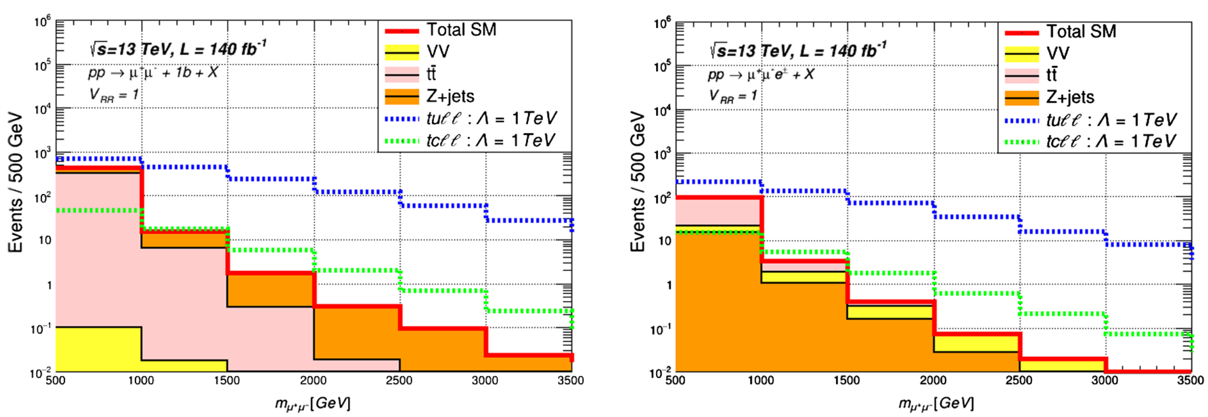


FIG. 5. Dimuon invariant mass distribution for the dilepton $pp \to \mu^+\mu^- + j_b + X$ (left) and trilepton $pp \to e\mu^+\mu^- + X$ (right) signal scenarios generated by the $tu\ell\ell$ and $tc\ell\ell$ vector operators with $V_{RR} = 1$ and $\Lambda = 1$ TeV. This is overlaid with the SM stacked $VV$, $t\bar{t}$ and $Z + \text{jets}$ background processes.

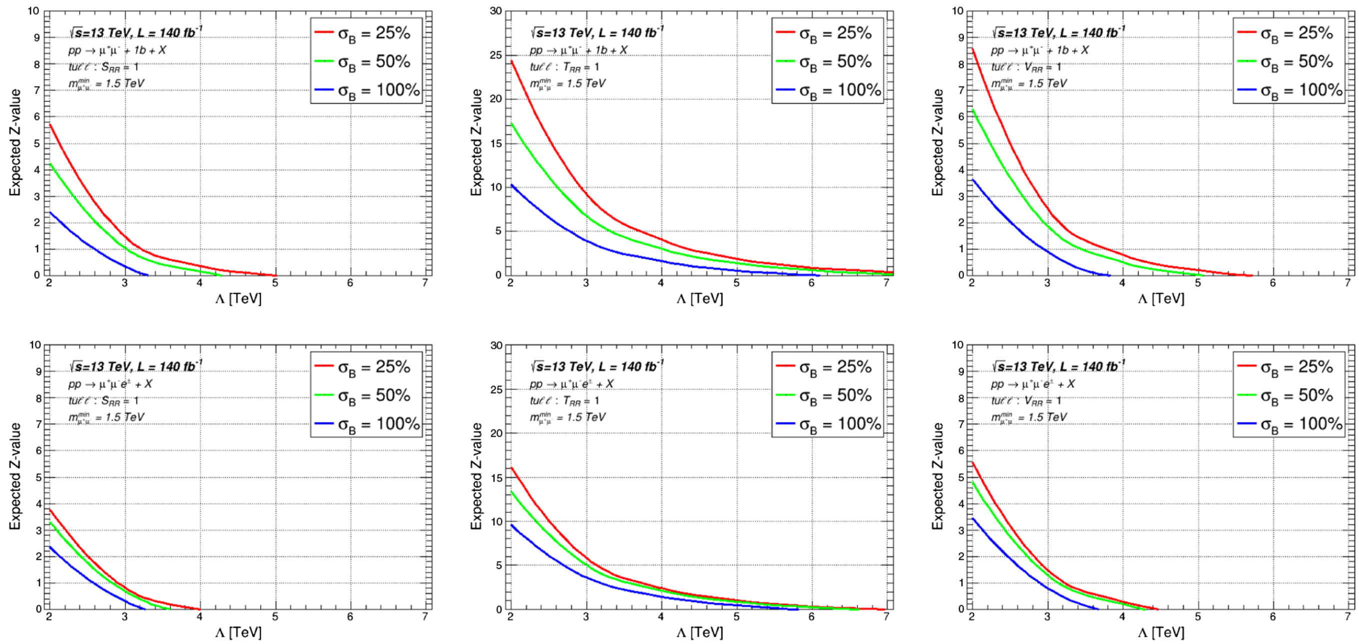


FIG. 6. Expected $Z$-value for the signal hypotheses varied with respect to the scale $\Lambda$, of the $tu\ell\ell$ scalar, tensor, and vector operators with $S_{RR} = 1$ (left), $T_{RR} = 1$ (middle) and $V_{RR} = 1$ (right), for an integrated luminosity of 140 fb$^{-1}$ and with $m^{\mathrm{min}}_{\mu^+\mu^-} = 1.5$ TeV. The $(\mu\mu 1b)$ and $(e\mu\mu)$ final state selections, $pp \to \mu^+\mu^- + j_b + X$ (upper) and $pp \to e\mu^+\mu^- + X$ (bottom), respectively, are presented.

### C. Results: Sensitivity and bounds

For a sensitivity study (i.e., placing a bound on the NP scale $\Lambda$), we calculated the $p$-value for each signal and background hypothesis using the BinomialExpP function by RooFit [142]. We calculate the $p$-value of the background-only and background + signal hypotheses for each point and then perform a $CL_s$ [143] test to determine the 95% confidence level (CL) exclusion values for $\Lambda$. We then find an optimized selection of a minimum OS dimuon invariant mass cut, $m^{\mathrm{min}}_{\mu\mu}$, which yields the best limit on $\Lambda$ in each channel, where at least one expected event was demanded for each one of the signal hypotheses.

The expected $Z$-value, which is defined as the number of standard deviations from the background-only hypothesis given a signal yield and background uncertainty, is calculated by the BinomialExpZ function by RooFit [142]. Examples of the expected $Z$-value from the trilepton signal are plotted in Fig. 6, as a function of $\Lambda$ for the case of the $tu\ell\ell$ operator and for several values of the relative overall uncertainty, $\sigma_B = 25\%,\ 50\%,\ 100\%$, with the currently available integrated luminosity of 140 fb$^{-1}$. Clearly, our results depend on the relative uncertainty. Furthermore, the relative uncertainties for the $(e\mu\mu)$ and $(\mu\mu 1b)$ signal selections may be different and that can determine which of the two is more adequate for searching for the 4-Fermi signal scenarios discussed in this paper. Keeping that in mind, we analyze both the $(e\mu\mu)$ and $(\mu\mu 1b)$ signal channels and choose a benchmark value of $\sigma_B = 25\%$ (see, e.g., [117]) for both of them, assuming that the signal uncertainty is included within $\sigma_B$.[10]

In Tables VIII–IX we present the expected 95% CL bounds on the scale $\Lambda$ of the $tull$ and $tcll$ operators, for the 3 different signal scenarios: $S_{RR} = 1$, $T_{RR} = 1$, and $V_{RR} = 1$. The 95% CL bounds on the scale of the $tu\ell\ell$ operator are also depicted in Fig. 7, for the optimized $m^{\mathrm{min}}_{\mu^+\mu^-}$ selection which yields the best expected limit for each case, along with the $\pm 1\sigma$ and $\pm 2\sigma$ bands, as explained below. As mentioned above, the two integrated luminosity scenarios $\mathcal{L} = 140$ and 3000 fb$^{-1}$ are considered. An upper cut of $m^{\mathrm{max}}_{\mu^+\mu^-} = 5$ TeV and $m^{\mathrm{max}}_{\mu^+\mu^-} = 3$ TeV were applied on the OSSF dimuons in the $tu\ell\ell$ and $tc\ell\ell$ cases, respectively, in order to be within the EFT validity regime, as discussed above. We note, though, that the 95% CL bounds reported here are rather mildly sensitive to $m^{\mathrm{max}}_{\mu^+\mu^-}$, as illustrated in Fig. 8 for the $tu\ell\ell$ and $tc\ell\ell$ scalar ($S_{RR}$) and tensor operators ($T_{RR}$).

### D. Results: Discovery potential

An estimate of the discovery potential can be inferred from the expected $Z$-values mentioned above; in particular, $Z = 5$ corresponds to a $5\sigma$ discovery. Once again, as a benchmark selection, we assume that the relative overall uncertainty is 25% and in Tables X–XI we list the expected

[10]We note that the statistical uncertainty from the event generator is of $\mathcal{O}(1\%)$ and is considered within this approximation.

TABLE VIII. Expected maximum 95% CL sensitivity ranges to the scale $\Lambda$, $\Lambda_{\rm min}(95\%CL)$, of the $tu\ell\ell$ and $tc\ell\ell$ 4-Fermi operators, obtained via the dilepton $(\mu\mu 1b)$ signal $pp \to \mu^+\mu^- + j_b + X$ with the corresponding optimal $m^{\rm min}_{\mu^+\mu^-}$ selection. An upper selection on the dimuon invariant mass of $m^{\rm max}_{\mu^+\mu^-} = 3, 5$ TeV was applied in the $tc\ell\ell$, $tu\ell\ell$ cases, respectively. Results are shown for the 3 signal scenarios of each operator: $S_{RR} = 1$, $T_{RR} = 1$, $V_{RR} = 1$. See also text and caption of Fig. 7.

| | Expected bounds $\Lambda_{\rm min}(95\%CL)$ [TeV]; $(\mu\mu 1b)$: $pp \to \mu^+\mu^- + j_b + X$ | | | | |
|---|---|---|---|---|---|
| | Operator | $\boldsymbol{tu\mu\mu}$ 4-Fermi case | | $\boldsymbol{tc\mu\mu}$ 4-Fermi case | |
| | Coupling | $m^{\rm min}_{\mu^+\mu^-}$ [GeV] | $\Lambda_{\rm min}(95\%CL)$ [TeV] | $m^{\rm min}_{\mu^+\mu^-}$ [GeV] | $\Lambda_{\rm min}(95\%CL)$ [TeV] |
| $\mathcal{L} = 140$ fb$^{-1}$ | $S_{RR} = 1$ | 1500 | $2.8^{+0.1}_{-0.1}$ | 1000 | $1.0^{+0.1}_{-0.1}$ [EFT?] |
| | $T_{RR} = 1$ | | $5.0^{+0.1}_{-0.2}$ | | $1.8^{+0.1}_{-0.1}$ |
| | $V_{RR} = 1$ | | $3.2^{+0.1}_{-0.1}$ | | $1.1^{+0.1}_{-0.1}$ |
| $\mathcal{L} = 3000$ fb$^{-1}$ | $S_{RR} = 1$ | 2000 | $4.1^{+0.1}_{-0.2}$ | 1500 | $1.3^{+0.1}_{-0.1}$ [EFT?] |
| | $T_{RR} = 1$ | | $7.1^{+0.3}_{-0.3}$ | | $2.4^{+0.1}_{-0.1}$ |
| | $V_{RR} = 1$ | | $4.7^{+0.2}_{-0.2}$ | | $1.5^{+0.1}_{-0.1}$ [EFT?] |

TABLE IX. Same as Table VIII but for the $(e\mu\mu)$ signal $pp \to e\mu^+\mu^- + X$.

| | Expected bounds $\Lambda_{\rm min}(95\%CL)$ [TeV]; $(e\mu\mu)$: $pp \to e\mu^+\mu^- + X$ | | | | |
|---|---|---|---|---|---|
| | Operator | $\boldsymbol{tu\mu\mu}$ 4-Fermi case | | $\boldsymbol{tc\mu\mu}$ 4-Fermi case | |
| | Coupling | $m^{\rm min}_{\mu^+\mu^-}$ [GeV] | $\Lambda_{\rm min}(95\%CL)$ [TeV] | $m^{\rm min}_{\mu^+\mu^-}$ [GeV] | $\Lambda_{\rm min}(95\%CL)$ [TeV] |
| $\mathcal{L} = 140$ fb$^{-1}$ | $S_{RR} = 1$ | 1500 | $2.3^{+0.0}_{-0.1}$ | 1000 | $0.9^{+0.0}_{-0.0}$ [EFT?] |
| | $T_{RR} = 1$ | | $4.1^{+0.1}_{-0.1}$ | | $1.7^{+0.1}_{-0.1}$ |
| | $V_{RR} = 1$ | | $2.7^{+0.0}_{-0.1}$ | | $1.1^{+0.0}_{-0.0}$ |
| $\mathcal{L} = 3000$ fb$^{-1}$ | $S_{RR} = 1$ | 1500 | $3.5^{+0.1}_{-0.1}$ | 1000 | $1.1^{+0.1}_{-0.1}$ |
| | $T_{RR} = 1$ | | $6.3^{+0.2}_{-0.3}$ | | $2.1^{+0.1}_{-0.1}$ |
| | $V_{RR} = 1$ | | $4.1^{+0.1}_{-0.2}$ | | $1.3^{+0.1}_{-0.1}$ |

$5\sigma$ discovery potential, $\Lambda(5\sigma)$, for the 3 different signal scenarios: $S_{RR} = 1$, $T_{RR} = 1$, $V_{RR} = 1$ of both the $tu\ell\ell$ and $tc\ell\ell$ 4-Fermi operators, via the $(\mu\mu 1b)$ and $(e\mu\mu)$ signal selections, respectively. Results are again shown for the two integrated luminosity cases corresponding to the currently accumulated LHC data and the planned HL-LHC luminosity. We see, e.g., that a $5\sigma$ discovery of the $tu\ell\ell$ tensor interactions is possible within the current LHC accumulated data if $\Lambda \lesssim 3.7$ TeV with the $(\mu\mu 1b)$ selection and $\Lambda \lesssim 3$ TeV in the trilepton $(e\mu\mu)$ case.

### E. Results: Sensitivity at a future 27 and 100 TeV hadron colliders

We have also extended our study to future hadron machines; specifically, to the sensitivity of a 27 TeV and a 100 TeV proton-proton collider to the $tu_i\ell\ell$ operators, for which we have assumed a total integrated luminosity of 15000 fb$^{-1}$ [144] and 20000 fb$^{-1}$ [145], respectively. The expected 95% CL bounds for the higher energy proton-proton colliders are presented in Fig. 9, where we show the 95% CL upper bounds on the scale of the $tu\ell\ell$ and $tc\ell\ell$ 4-Fermi operators for the 3 signal scenarios $S_{RR} = 1$, $T_{RR} = 1$ and $V_{RR} = 1$. Here also, the expected bounds are presented for the optimized $m^{\rm min}_{\mu^+\mu^-}$ selections and an upper cut on the OSSF muons of $m^{\rm max}_{\mu^+\mu^-} = 10$, 30 TeV for the 27 TeV and 100 TeV cases, respectively, and with a $25\%(1\sigma)$ relative uncertainty.

We see from Fig. 9 that a 27 TeV (100 TeV) proton collider is expected to be sensitive (at 95% CL) to $\Lambda \gtrsim$ 8–13 TeV ($\Lambda \gtrsim$ 19–37 TeV) for the $tu\ell\ell$ operator and to $\Lambda \gtrsim$ 3–5 TeV ($\Lambda \gtrsim 9 - 16$ TeV) for the $tc\ell\ell$ one. This should be compared with the expected reach at other future colliders, such as the proposed Circular Electron Positron Collider (CEPC, see, e.g., [146]) and Compact Linear Collider (CLIC, see, e.g., [147] and references therein) $e^+e^-$-machines and the $ep$ Large Hadron-Electron Collider (LHeC, see. e.g., [148]). For example, it was shown in [149,150] that the CEPC and CLIC machines, respectively, will be sensitive to scales of the $tuee$ and $tcee$ scalar, vector and tensor operators in the range $\Lambda \sim 5$–10 TeV, depending on the center of mass energy of these future $ee$ machines. For the $tuee$ 4-Fermi terms this is comparable to the reach expected at the HL-LHC via our di- and trilepton signals (as shown above), whereas for the $tcee$

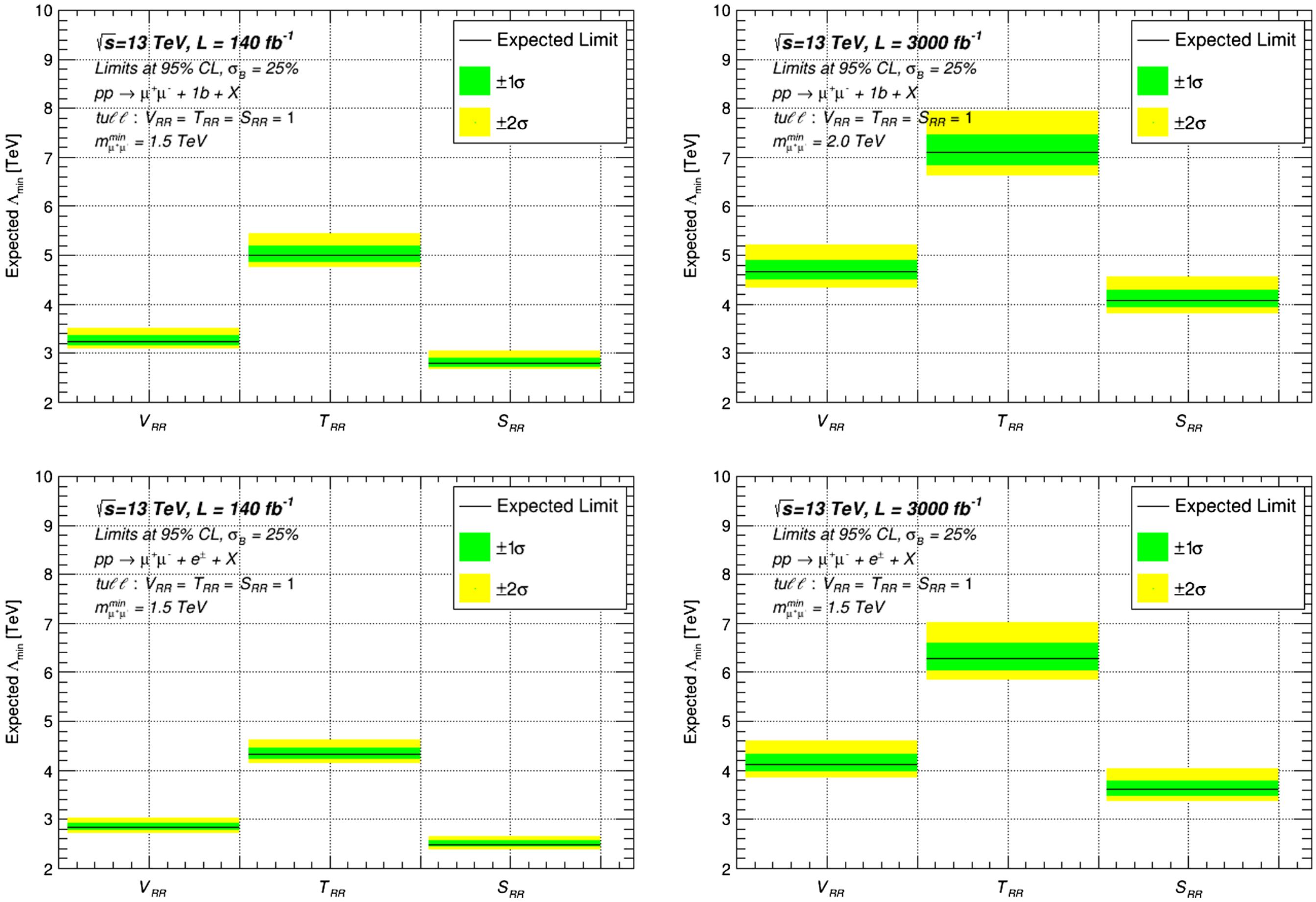


FIG. 7. Expected 95% CL upper limit on $\Lambda$, $\Lambda_{\text{min}}(95\%CL)$, of the $tu\ell\ell$ operator for 3 signal scenarios: $S_{RR}=1$, $T_{RR}=1$, and $V_{RR}=1$, and total integrated luminosities of 140 fb$^{-1}$ (left) and 3000 fb$^{-1}$ (right). The $(\mu\mu 1b)$ and $(e\mu\mu)$ final states selection are presented in the upper and lower plots, respectively. For all cases $m^{\text{max}}_{\mu^+\mu^-}=5$ TeV and the optimal $m^{\text{min}}_{\mu^+\mu^-}$ selections were used (see also Tables VIII–IX). Also, for all cases the overall uncertainty is chosen to be 25% at $1\sigma$ as explained in the text.

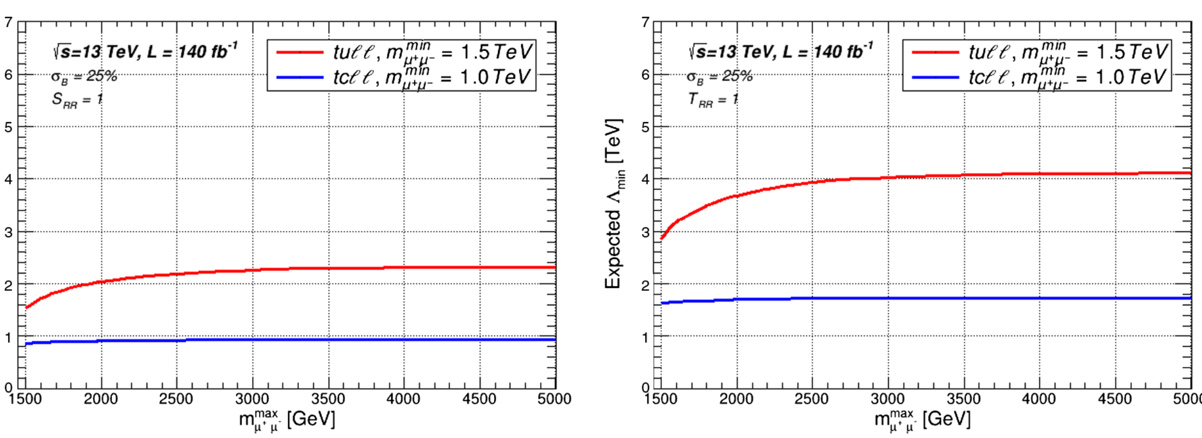


FIG. 8. Expected 95% CL upper limit on the scale $\Lambda$ of the $tu\ell\ell$ and $tc\ell\ell$ operators for the $S_{RR}$ (left) and $T_{RR}$ signal scenarios, as a function of the upper invariant mass selection, $m^{\text{max}}_{\mu^+\mu^-}$. Results are shown for a total integrated luminosity of 140 fb$^{-1}$. In both cases we assume 25% background uncertainty at $1\sigma$.

TABLE X. Expected discovery potential for the scale of NP Λ, of the $tu\ell\ell$ and $tc\ell\ell$ 4-Fermi operators, obtained via the dilepton $(\mu\mu 1b)$ signal $pp \to \mu^+\mu^- + j_b + X$ with the corresponding optimal $m^{\rm min}_{\mu^+\mu^-}$ selection. An upper selection on the dimuon invariant mass of $m^{\rm max}_{\mu^+\mu^-} = 3$, 5 TeV was applied in the $tc\ell\ell$, $tu\ell\ell$ cases, respectively. Results are shown for the 3 signal scenarios of each operator: $S_{RR} = 1$, $T_{RR} = 1$, $V_{RR} = 1$.

| | Expected discovery potential $\Lambda(5\sigma)$ [TeV]; $(\mu\mu 1b)$: $pp \to \mu^+\mu^- + j_b + X$ | | | | |
|---|---|---|---|---|---|
| | Operator | $tu\mu\mu$ 4-Fermi case | | $tc\mu\mu$ 4-Fermi case | |
| | Coupling | $m^{\rm min}_{\mu^+\mu^-}$ [GeV] | $\Lambda(5\sigma)$ [TeV] | $m^{\rm min}_{\mu^+\mu^-}$ [GeV] | $\Lambda(5\sigma)$ [TeV] |
| $\mathcal{L} = 140$ fb$^{-1}$ | $S_{RR} = 1$ | 1500 | 2.1 | | 0.7 [EFT?] |
| | $T_{RR} = 1$ | | 3.7 | 1000 | 1.4 |
| | $V_{RR} = 1$ | | 2.4 | | 0.9 [EFT?] |
| $\mathcal{L} = 3000$ fb$^{-1}$ | $S_{RR} = 1$ | 2000 | 3.1 | 1500 | 1.0 [EFT?] |
| | $T_{RR} = 1$ | | 5.3 | | 1.8 |
| | $V_{RR} = 1$ | | 3.5 | | 1.1 [EFT?] |

TABLE XI. Same as Table X but for the $(e\mu\mu)$ signal $pp \to e\mu^+\mu^- + X$.

| | Coupling | $m^{\rm min}_{\mu^+\mu^-}$ [GeV] | $\Lambda(5\sigma)$ [TeV] | $m^{\rm min}_{\mu^+\mu^-}$ [GeV] | $\Lambda(5\sigma)$ [TeV] |
|---|---|---|---|---|---|
| | Expected discovery potential $\Lambda(5\sigma)$ [TeV]; $(e\mu\mu)$: $pp \to e\mu^+\mu^- + X$ | | | | |
| | Operator | $tu\mu\mu$ 4-Fermi case | | $tc\mu\mu$ 4-Fermi case | |
| $\mathcal{L} = 140$ fb$^{-1}$ | $S_{RR} = 1$ | 1500 | 1.7 | 1000 | 0.7 [EFT?] |
| | $T_{RR} = 1$ | | 3.0 | | 1.3 |
| | $V_{RR} = 1$ | | 1.9 | | 0.8 [EFT?] |
| $\mathcal{L} = 3000$ fb$^{-1}$ | $S_{RR} = 1$ | 1500 | 2.7 | 1000 | 0.9 [EFT?] |
| | $T_{RR} = 1$ | | 4.7 | | 1.6 |
| | $V_{RR} = 1$ | | 3.0 | | 1.0 [EFT?] |

operators this is about an order of magnitude better than what we found for the HL-LHC setup, while it is comparable to the expected sensitivity at the HE-LHC (i.e., a 27 or 100 TeV LHC upgrade, see Fig. 9). On the other hand, the sensitivity of the LHeC machine to the $tuee$ and $tcee$ operators via the single-top $ep \to et$ production channel that was studied in [150], is comparable to what we find for the current LHC data with 140 fb$^{-1}$ of data.

We note, though, that these future $ee$ and $ep$ machines are sensitive only to the $tu_iee$ 4-Fermi operators, as opposed to the LHC which, as we show, can probe also the dimuon $tu_i\mu\mu$ operators via our di- and trilepton signals.

### F. Results: Final remarks

To conclude this section, let us recapitulate some of the salient features of our findings and also further comment on the potential richness of the multilepton signals considered above:

(i) The three lepton final states with an additional light and/or $b$-jet can be a useful probe for searching NP in general; their applicability is not restricted to FC process or to a SMEFT parametrization. These final states are rich in observables sensitive to deviations form the SM; some interesting examples are a forward-backward asymmetry, energy asymmetry and triple correlation asymmetries, which can be readily constructed from the available energies and the 4-momenta of the charged leptons along with the 4-momenta of the light and/or $b$-jet in the trilepton final state [19].

(ii) For the SMEFT parameterization of FC effects, both the di- and trilepton signals are significantly more sensitive to the $tu\ell\ell$ than to the $tc\ell\ell$ 4-Fermi interaction as a result of the larger $u$-quark content in the colliding protons and the importance of the $ug$ fusion diagrams in Fig. 2.

(iii) An extra selection of exactly one $b$-tagged jet on the dilepton signature can yield a significantly better sensitivity to the scale of the underlying FC NP (see Tables VIII–XI).

(iv) Since there are no significant SM × NP interference effects for the FC EFT we consider, the sensitivity and reach for the other 4-Fermi vector currents, $V_{LL}$, $V_{RL}$ and $V_{LR}$ will be identical to that of $V_{RR}$ (which is the one studied above).

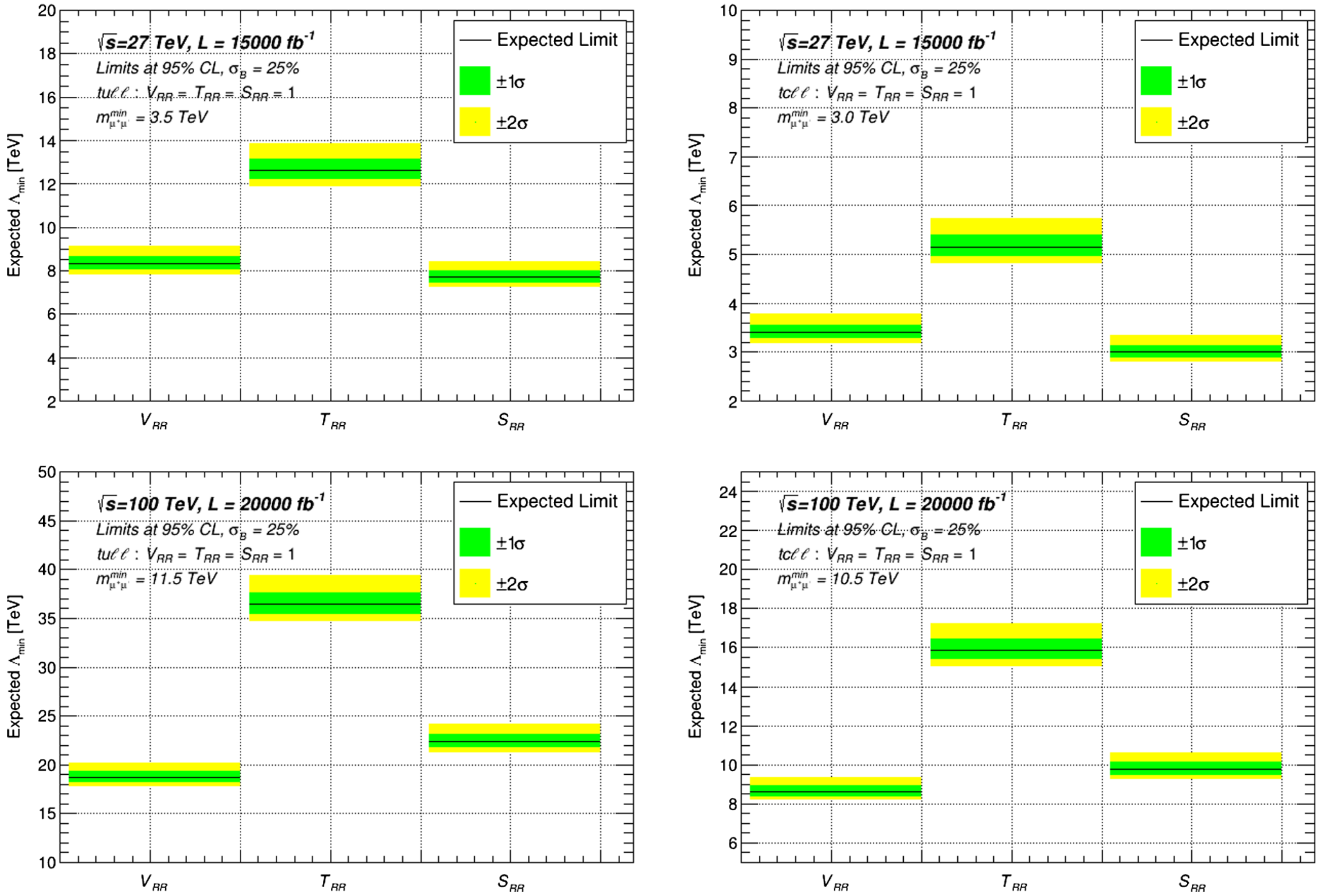


FIG. 9. Expected 95% CL upper limit on $\Lambda$ of the $tu\ell\ell$ (left) and $tc\ell\ell$ (right) operators for center-of-mass energy of 27 TeV (upper plots) and 100 TeV (lower plots), for 3 signal scenarios: $S_{RR} = 1$, $T_{RR} = 1$, and $V_{RR} = 1$. The total integrated luminosity is 15000 fb$^{-1}$ for the 27 TeV machine and 20000 fb$^{-1}$ for 100 TeV one. Results are shown with 25% overall relative uncertainty at $1\sigma$ and with $m^{\rm min}_{\mu^+\mu^-}$ selections as indicated. See also text.

## VI. LEPTON FLAVOR NONUNIVERSALITY

As mentioned earlier, the di- and trilepton signals can also be used to study possible LFNU effects in the FC $tu_i\ell\ell$ 4-Fermi operators from lepton nonuniversal effects in the underlying heavy theory, e.g., LFNU couplings of a heavy vector or heavy scalar to the SM leptons.[11] Following the work in [119], we can define generic LFNU "tests" for our single-top + dilepton signals (3), normalized to the dielectron channels, as follows:

$$T_{t\ell\ell_0} = \frac{\sigma_{(t\ell\ell)_0}}{\sigma_{(tee)_0}}, \qquad T_{t\ell\ell_1} = \frac{\sigma_{(t\ell\ell)_1}}{\sigma_{(tee)_1}}; \tag{19}$$

or, more generally, for our inclusive di- and trilepton signals:

$$T^{1b}_{\ell\ell} = \frac{N(\ell\ell 1b)}{N(ee1b)}, \qquad T^{\ell'/\ell''}_{\ell\ell} = \frac{N(\ell'\ell\ell)}{N(\ell''ee)}, \tag{20}$$

where $N(\ell\ell 1b)$ and $N(\ell'\ell\ell)$ are the number of $pp \to \ell^+\ell^- + j_b + X$ and $pp \to \ell'\ell^+\ell^- + X$ events, respectively. An example of an interesting test of LFNU signals is provided by $T^{\mu/e}_{\mu\mu}$ that measures a possible difference in the $tu_i\mu\mu$ and $tu_iee$ contact interactions. With a selection $m^{\rm min}_{\ell\ell} > 1000$ GeV (ensuring, as shown above, negligible SM background to the NP trilepton signals), we have:

$$T^{\mu/e}_{\mu\mu} = \frac{N(\mu\mu\mu)}{N(eee)} \approx \frac{\Lambda^4_\mu}{\Lambda^4_e}, \tag{21}$$

where here $\Lambda_\ell$ denote the scale of the $tu\ell\ell$ operator.

In Fig. 10 we plot the regions in the $\Lambda_\mu - \Lambda_e$ plane where LFU can be tested with $T^{\mu/e}_{\mu\mu}$, depending on the uncertainty ($\delta T$) in its measurement. We also show in Fig. 10 the size of

[11]The LFNU effects we consider correspond to differences in the $tuee$, $tu\mu\mu$, and $tu\tau\tau$ couplings, and not possible $tue\mu$ interactions.

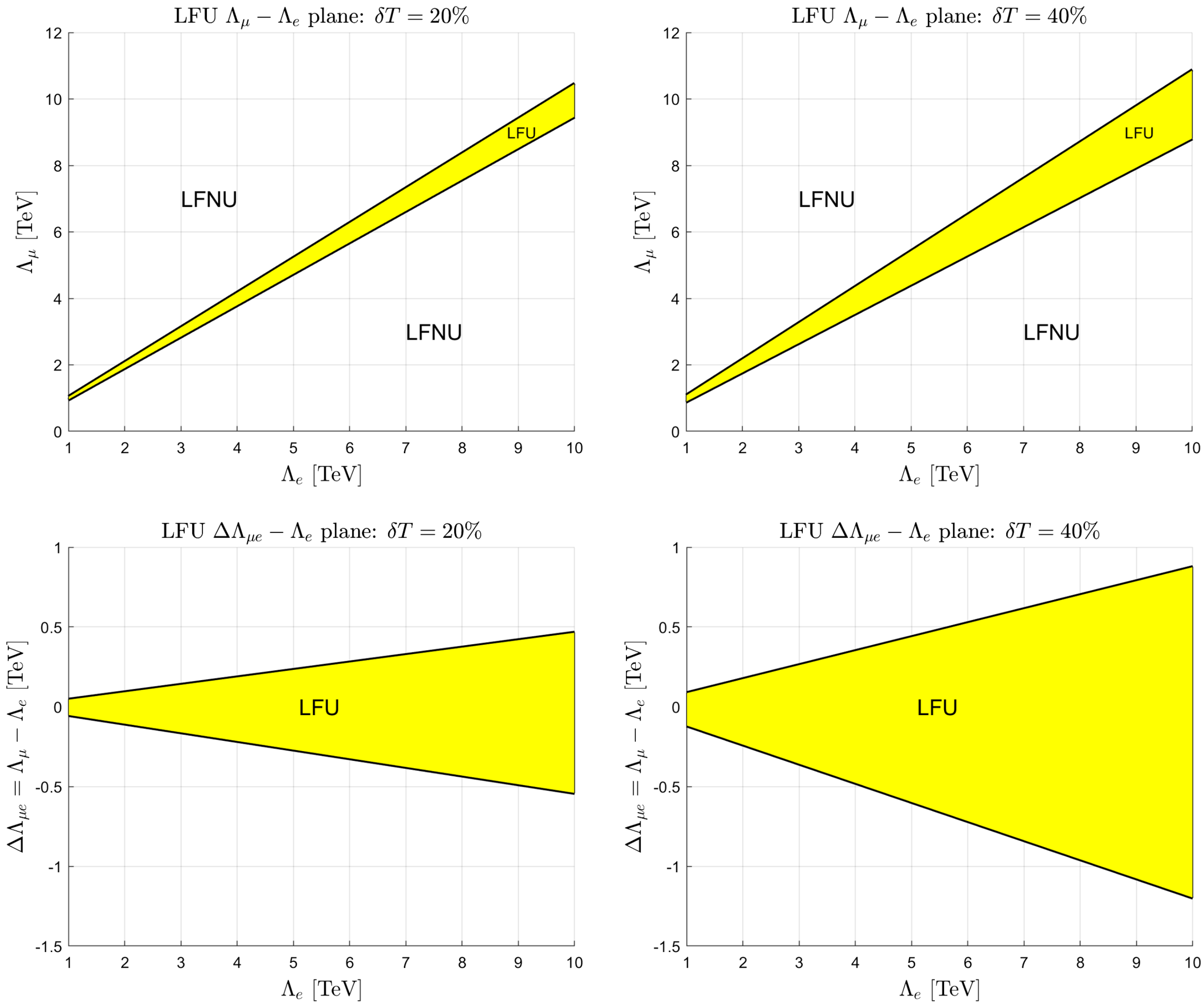


FIG. 10. Lepton flavor universal (LFU) regions (yellow shaded) in the $\Lambda_\mu - \Lambda_e$ and $\Lambda_{\mu e} - \Lambda_e$ planes, where $\Lambda_{\mu e} \equiv \Lambda_\mu - \Lambda_e$. The areas outside the yellow shaded areas are where LFU is violated. Two cases are shown: a 20% (left plots) and 40% (right plots) uncertainty in the measurement of the LFU T-test in (21). See also text.

$\Delta\Lambda_{\mu e} = \Lambda_\mu - \Lambda_e$ splitting required for observing LFNU effects. We see, e.g., that $|\Delta\Lambda_{\mu e}| \gtrsim 0.2$ TeV will yield a measurable LFNU signal if $T^{\mu/e}_{\mu\mu}$ can be measured to a 20% precision.[12]

## VII. SUMMARY

We have considered the effects of 4-Fermi $tu_i\ell\ell$ flavor changing interactions ($u_i \in u, c$) in the top-quark sector, which can be generated from different types of underlying heavy physics containing e.g., heavy scalars and/or vectors. We showed that these higher-dimensional FCNC top interactions can lead to new single-top + dilepton signals at the LHC via $pp \to t\ell^+\ell^-$ and $pp \to t\ell^+\ell^- + j$ ($j =$ light jet), which can be efficiently probed via the dilepton + $b$-jet $pp \to \ell^+\ell^- + j_b + X$ signal and/or in trilepton $pp \to \ell'\ell^+\ell^- + X$ events, containing opposite-sign same-flavor (OSSF) dileptons, e.g., $pp \to e\mu^+\mu^- + X$, if the NP involves the $tu_i\mu\mu$ contact terms and the top decays via $t \to bW \to be\nu_e$.

We have studied in some detail the SM background to these di- and trilepton signatures, which is dominated by $pp \to t\bar{t}, Z +$ jets, $WZ$ and showed that an excellent separation between the NP signals and the background can be obtained with a selection of events with high OSSF

[12]Note that ratio observables such as in (20) and (21) provide more reliable probes of NP, since they potentially minimize the effects of the theoretical uncertainties involved in the calculation of the corresponding cross sections [119].

dileptons invariant mass $m_{\ell^+\ell^-}^{\rm min}({\rm OSSF}) > 1$ TeV. The high invariant mass selection on the OSSF dileptons also allows to isolate the FC $tu_i\ell\ell$ 4-Fermi dynamics from other types of NP, e.g., anomalous FC $tu_iZ$ terms, that may also contribute to the same di- and trilepton signals, but with on-$Z$ peak OSSF dileptons. We also find that an additional selection of a single $b$-tagged jet is useful for tracking the top-quark decay in these events and, in the dilepton signal case $pp \to \ell^+\ell^- + j_b + X$, it significantly improves the sensitivity to the scale of these FC $tu_i\ell\ell$ operators.

We have shown that the current $\mathcal{O}(1)$ TeV bounds on the scale of these $tu\ell\ell$ and $tc\ell\ell$ FC 4-Fermi interactions (from LEP2 and from $pp \to t\bar{t}$ followed by $t \to \ell^+\ell^- j$) can be appreciably improved. For example, 95% CL bounds of $\Lambda \lesssim 5(3.2)$ TeV are expected on the scale of a tensor (vector) $tu\mu\mu$ interaction, already with the current $\sim 140$ fb$^{-1}$ of LHC data, via the dimuon $pp \to \mu^+\mu^- + j_b + X$ signal; this is an improvement by a factor of 3–5 with respect to the current bounds on these operators. The expected reach at the HL-LHC with 3000 fb$^{-1}$ of data is $\Lambda \lesssim 7.1(4.7)$ TeV for the tensor(vector) FC $tu\ell\ell$ 4-Fermi interactions and $\Lambda \lesssim 2.4(1.5)$ TeV for the corresponding $tc\mu\mu$ operators. We have considered the consistency of these bounds with restrictive requirements for the domain of validity of the EFT prescription and imposed the relevant EFT-validity criteria accordingly.

We have also considered the potential sensitivity of higher energy 27 and 100 TeV proton-proton colliders to the $tu\ell\ell$ and $tc\ell\ell$ 4-Fermi operators and found that a 27 TeV machine will be able to probe scales of $\Lambda \lesssim 8-15$ TeV and $\Lambda \gtrsim 4-5$ TeV for the scalar, vector and tensor $tu\ell\ell$ and $tc\ell\ell$ operators, respectively. Likewise, a 100 TeV proton collider will be sensitive to scales of $\Lambda \gtrsim 20-35$ TeV and $\Lambda \gtrsim 9-15$ TeV for the $tu\ell\ell$ and $tc\ell\ell$ operators.

We furthermore explored potential searches for lepton nonuniversal effects that can be performed with our multi-lepton signals, finding e.g., that if the typical scale of these 4-Fermi $tu_i\ell\ell$ operators is around 5 TeV, then a separation of more than $\mathcal{O}(0.5)$ TeV between the scales of the $tu_i\mu\mu$ and $tu_iee$ 4-Fermi terms, may be distinguishable via our di- and trilepton signatures, indicating that the underlying heavy physics is lepton nonuniversal.

Finally, we end with a cautionary remark. A positive signal through these tests does not necessarily mean that the underlying new physics is flavor changing, but rather, it means that it may be so and further studies will be needed for confirmation.

## ACKNOWLEDGMENTS

The work of A. S. was supported in part by the U.S. DOE Contract No. DE-SC0012704.


[1] G. Eilam, J. L. Hewett, and A. Soni, Rare decays of the top quark in the standard and two Higgs doublet models, Phys. Rev. D **44**, 1473 (1991); Erratum, Phys. Rev. D **59**, 039901 (1998).

[2] W. Buchmuller and M. Gronau, Flavor changing $Z^0$ decays, Phys. Lett. B **220**, 641 (1989).

[3] H. Fritzsch, T quarks may decay into $Z$ Bosons and Charm, Phys. Lett. B **224**, 423 (1989).

[4] J. L. Diaz-Cruz, R. Martinez, M. A. Perez, and A. Rosado, Flavor changing radiative decay of Thf T quark, Phys. Rev. D **41**, 891 (1990).

[5] B. Dutta-Roy, B. A. Irwin, B. Margolis, J. Robinson, H. D. Trottier, and C. Hamazaoui, Threshold Enhancement and the Flavor Changing Electromagnetic Vertex, Phys. Rev. Lett. **65**, 827 (1990).

[6] J. L. Diaz-Cruz and G. Lopez Castro, *CP* violation and FCNC with the top quark, Phys. Lett. B **301**, 405 (1993).

[7] B. Mele, S. Petrarca, and A. Soddu, A new evaluation of the $t->$ cH decay width in the standard model, Phys. Lett. B **435**, 401 (1998).

[8] I. Baum, G. Eilam, and S. Bar-Shalom, Scalar flavor changing neutral currents and rare top quark decays in a two Higgs doublet model 'for the top quark', Phys. Rev. D **77**, 113008 (2008).

[9] K. Agashe, G. Perez, and A. Soni, Flavor structure of warped extra dimension models, Phys. Rev. D **71**, 016002 (2005).

[10] K.-F. Chen, W.-S. Hou, C. Kao, and M. Kohda, When the Higgs meets the top: Search for $t \to ch^0$ at the LHC, Phys. Lett. B **725**, 378 (2013).

[11] A. Axelrod, Flavor changing $Z^0$ decay and the top quark, Nucl. Phys. **B209**, 349 (1982).

[12] M. Clements, C. Footman, A. S. Kronfeld, S. Narasimhan, and D. Photiadis, Flavor changing decays of the $Z^0$, Phys. Rev. D **27**, 570 (1983).

[13] G. Eilam, Production of a single heavy quark in $e^+e^-$ collisions, Phys. Rev. D **28**, 1202 (1983).

[14] C.-H. Chang, X.-Q. Li, J.-X. Wang, and M.-Z. Yang, The production of t anti-c or anti-t c quark pair by $e^+e^-$ collision based on the standard model and its extensions, Phys. Lett. B **313**, 389 (1993).

[15] C.-S. Huang, X.-H. Wu, and S.-H. Zhu, Top charm associated production at high-energy $e^+e^-$ colliders in standard model, Phys. Lett. B **452**, 143 (1999).

[16] D. Atwood, L. Reina, and A. Soni, Probing flavor changing top—charm—scalar interactions in $e^+e^-$ collisions, Phys. Rev. D **53**, 1199 (1996).

[17] K. Agashe, G. Perez, and A. Soni, Collider signals of top quark flavor violation from a warped extra dimension, Phys. Rev. D **75**, 015002 (2007).

[18] W.-S. Hou, G.-L. Lin, and C.-Y. Ma, Flavor changing neutral Higgs couplings and top charm production at next linear collider, Phys. Rev. D **56**, 7434 (1997).

[19] D. Atwood, S. Bar-Shalom, G. Eilam, and A. Soni, *CP* violation in top physics, Phys. Rep. **347**, 1 (2001).

[20] R. Aaij *et al.*, Differential branching fractions and isospin asymmetries of $B \to K^{(*)}\mu^+\mu^-$ decays, J. High Energy Phys. 06 (2014) 133.

[21] R. Aaij *et al.*, Test of Lepton Universality using $B^+ \to K^+\ell^+\ell^-$ Decays, Phys. Rev. Lett. **113**, 151601 (2014).

[22] R. Aaij *et al.*, Test of lepton universality with $B^0 \to K^{*0}\ell^+\ell^-$ decays, J. High Energy Phys. 08 (2017) 055.

[23] R. Aaij *et al.*, Angular analysis and differential branching fraction of the decay $B_s^0 \to \phi\mu^+\mu^-$, J. High Energy Phys. 09 (2015) 179.

[24] R. Aaij *et al.*, Angular analysis of the $B^0 \to K^{*0}\mu^+\mu^-$ decay using 3 $\mathrm{fb}^{-1}$ of integrated luminosity, J. High Energy Phys. 02 (2016) 104.

[25] S. Wehle *et al.*, Lepton-Flavor-Dependent Angular Analysis of $B \to K^*\ell^+\ell^-$, Phys. Rev. Lett. **118**, 111801 (2017).

[26] A. Abdesselam *et al.*, Angular analysis of $B^0 \to K^*(892)^0\ell^+\ell^-$, in *Proceedings, LHCSki 2016—A First Discussion of 13 TeV Results: Obergurgl, Austria, April 10–15, 2016* (2016) [arXiv:1604.04042].

[27] The ATLAS Collaboration, Angular analysis of $B_d^0 \to K^*\mu^+\mu^-$ decays in $pp$ collisions at $\sqrt{s} = 8$ TeV with the ATLAS detector, ATLAS-CONF-2017-023 (2017).

[28] CMS Collaboration, Measurement of the $P_1$ and $P_5'$ angular parameters of the decay $\mathrm{B}^0 \to \mathrm{K}^{*0}\mu^+\mu^-$ in proton-proton collisions at $\sqrt{s} = 8$ TeV, CMS-PAS-BPH-15-008 (2017).

[29] S. Bifani, Status of new physics searches with $b \to s\ell^+\ell^-$ transitions @ LHCb, In *Proceedings, 52nd Rencontres de Moriond on Electroweak Interactions and Unified Theories: La Thuile, Italy, March 18-25, 2017* (2017), pp. 197–202 [arXiv:1705.02693].

[30] R. Aaij *et al.*, Search for Lepton-Universality Violation in $B^+ \to K^+\ell^+\ell^-$ Decays, Phys. Rev. Lett. **122**, 191801 (2019).

[31] A. Abdesselam *et al.*, Test of lepton flavor universality in $B \to K^*\ell^+\ell^-$ decays at Belle, arXiv:1904.02440.

[32] J. P. Lees *et al.*, Evidence for an Excess of $\bar{B} \to D^{(*)}\tau^-\bar{\nu}_\tau$ Decays, Phys. Rev. Lett. **109**, 101802 (2012).

[33] J. P. Lees *et al.*, Measurement of an excess of $\bar{B} \to D^{(*)}\tau^-\bar{\nu}_\tau$ decays and implications for charged Higgs bosons, Phys. Rev. D **88**, 072012 (2013).

[34] M. Huschle *et al.*, Measurement of the branching ratio of $\bar{B} \to D^{(*)}\tau^-\bar{\nu}_\tau$ relative to $\bar{B} \to D^{(*)}\ell^-\bar{\nu}_\ell$ decays with hadronic tagging at Belle, Phys. Rev. D **92**, 072014 (2015).

[35] S. Hirose *et al.*, Measurement of the $\tau$ Lepton Polarization and $R(D^*)$ in the Decay $\bar{B} \to D^*\tau^-\bar{\nu}_\tau$, Phys. Rev. Lett. **118**, 211801 (2017).

[36] R. Aaij *et al.*, Measurement of the Ratio of Branching Fractions $\mathcal{B}(\bar{B}^0 \to D^{*+}\tau^-\bar{\nu}_\tau)/\mathcal{B}(\bar{B}^0 \to D^{*+}\mu^-\bar{\nu}_\mu)$, Phys. Rev. Lett. **115**, 111803 (2015); Erratum, Phys. Rev. Lett. **115**, 159901 (2015).

[37] R. Aaij *et al.*, Measurement of the Ratio of the $B^0 \to D^{*-}\tau^+\nu_\tau$ and $B^0 \to D^{*-}\mu^+\nu_\mu$ Branching Fractions using Three-Prong $\tau$-Lepton Decays, Phys. Rev. Lett. **120**, 171802 (2018).

[38] R. Aaij *et al.*, Test of lepton flavor universality by the measurement of the $B^0 \to D^{*-}\tau^+\nu_\tau$ branching fraction using three-prong $\tau$ decays, Phys. Rev. D **97**, 072013 (2018).

[39] K. Adamczyk, Semitauonic $B$ decays at Belle/Belle II, in *Proceedings of 10th International Workshop on the CKM Unitarity Triangle (CKM 2018) Heidelberg, Germany, September 17-21, 2018* (2019) [arXiv:1901.06380].

[40] A. Abdesselam *et al.*, Measurement of $\mathcal{R}(D)$ and $\mathcal{R}(D^*)$ with a semileptonic tagging method, arXiv:1904.08794.

[41] S. Bifani, S. Descotes-Genon, A. Romero Vidal, and M.-H. Schune, Review of lepton universality tests in $B$ decays, J. Phys. G **46**, 023001 (2019).

[42] E. Alvarez, A. Juste, M. Szewc, and T. Vazquez Schroeder, Topping-up multilepton plus b-jets anomalies at the LHC with a $Z'$ boson, arXiv:2011.06514.

[43] S. Davidson, M. L. Mangano, S. Perries, and V. Sordini, Lepton flavour violating top decays at the LHC, Eur. Phys. J. C **75**, 450 (2015).

[44] M. Chala, J. Santiago, and M. Spannowsky, Constraining four-fermion operators using rare top decays, J. High Energy Phys. 04 (2019) 014.

[45] C. A. Gottardo, Search for charged lepton-flavour violation in top-quark decays at the LHC with the ATLAS detector, PhD thesis, University of Bonn (main), 2019.

[46] C. Degrande, F. Maltoni, K. Mimasu, E. Vryonidou, and C. Zhang, Single-top associated production with a $Z$ or $H$ boson at the LHC: The SMEFT interpretation, J. High Energy Phys. 10 (2018) 005.

[47] G. Durieux, F. Maltoni, and C. Zhang, Global approach to top-quark flavor-changing interactions, Phys. Rev. D **91**, 074017 (2015).

[48] N. P. Hartland, F. Maltoni, E. R. Nocera, J. Rojo, E. Slade, E. Vryonidou, and C. Zhang, A Monte Carlo global analysis of the standard model effective field theory: The top quark sector, J. High Energy Phys. 04 (2019) 100.

[49] G. Durieux, A. Irles, V. Miralles, A. Peñuelas, R. Pöschl, M. Perelló, and M. Vos, The electro-weak couplings of the top and bottom quarks—global fit and future prospects, J. High Energy Phys. 12 (2019) 098.

[50] T. M. P. Tait and C.-P. Yuan, Single top quark production as a window to physics beyond the Standard Model, Phys. Rev. D **63**, 014018 (2000).

[51] N. Kidonakis and A. Belyaev, FCNC top quark production via anomalous tqV couplings beyond leading order, J. High Energy Phys. 12 (2003) 004.

[52] I. Brivio, S. Bruggisser, F. Maltoni, R. Moutafis, T. Plehn, E. Vryonidou, S. Westhoff, and C. Zhang, O new physics, where art thou? A global search in the top sector, J. High Energy Phys. 02 (2020) 131.

[53] D. Barducci *et al.*, Interpreting top-quark LHC measurements in the standard-model effective field theory, arXiv: 1802.07237.

[54] F. Maltoni, L. Mantani, and K. Mimasu, Top-quark electroweak interactions at high energy, J. High Energy Phys. 10 (2019) 004.

[55] T. Neumann and Z. E. Sullivan, Off-shell single-top-quark production in the standard model effective field theory, J. High Energy Phys. 06 (2019) 022.
[56] C. Englert, M. Russell, and C. D. White, Effective field theory in the top sector: Do multijets help?, Phys. Rev. D **99**, 035019 (2019).
[57] C. Zhang, Single Top Production at Next-to-Leading Order in the Standard Model Effective Field Theory, Phys. Rev. Lett. **116**, 162002 (2016).
[58] F. Maltoni, K. Paul, T. Stelzer, and S. Willenbrock, Associated production of Higgs and single top at hadron colliders, Phys. Rev. D **64**, 094023 (2001).
[59] S. Biswas, E. Gabrielli, and B. Mele, Single top and Higgs associated production as a probe of the Htt coupling sign at the LHC, J. High Energy Phys. 01 (2013) 088.
[60] M. Farina, C. Grojean, F. Maltoni, E. Salvioni, and A. Thamm, Lifting degeneracies in Higgs couplings using single top production in association with a Higgs boson, J. High Energy Phys. 05 (2013) 022.
[61] F. Demartin, F. Maltoni, K. Mawatari, and M. Zaro, Higgs production in association with a single top quark at the LHC, Eur. Phys. J. C **75**, 267 (2015).
[62] L. Wu, Enhancing $thj$ production from top-Higgs FCNC couplings, J. High Energy Phys. 02 (2015) 061.
[63] W. Liu, H. Sun, X.-J. Wang, and X. Luo, Probing the anomalous FCNC top-Higgs Yukawa couplings at the large hadron electron collider, Phys. Rev. D **92**, 074015 (2015).
[64] Y.-B. Liu and Z.-J. Xiao, Searches for the FCNC couplings from top-Higgs associated production signal with $h \to \gamma\gamma$ at the LHC, Phys. Lett. B **763**, 458 (2016).
[65] Y.-B. Liu and Z.-J. Xiao, Searches for top-Higgs FCNC couplings via the Whj signal with $h \to \gamma\gamma$ at the LHC, Phys. Rev. D **94**, 054018 (2016).
[66] J.-F. Shen, Y.-Q. Li, and Y.-B. Liu, Searches for anomalous tqZ couplings from the trilepton signal of tZ associated production at the 14 TeV LHC, Phys. Lett. B **776**, 391 (2018).
[67] F. del Aguila, J. A. Aguilar-Saavedra, and L. Ametller, Z t and gamma t production via top flavor changing neutral couplings at the Fermilab Tevatron, Phys. Lett. B **462**, 310 (1999).
[68] H. Khanpour, S. Khatibi, M. Khatiri Yanehsari, and M. Mohammadi Najafabadi, Single top quark production as a probe of anomalous $tq\gamma$ and $tqZ$ couplings at the FCC-ee, Phys. Lett. B **775**, 25 (2017).
[69] N. Kidonakis, Higher-order corrections for $tZ$ production via anomalous couplings, Phys. Rev. D **97**, 034028 (2018).
[70] P. M. Ferreira, R. B. Guedes, and R. Santos, Combined effects of strong and electroweak FCNC effective operators in top quark physics at the CERN LHC, Phys. Rev. D **77**, 114008 (2008).
[71] B. H. Li, Y. Zhang, C. S. Li, J. Gao, and H. X. Zhu, Next-to-leading order QCD corrections to $tZ$ associated production via the flavor-changing neutral-current couplings at hadron colliders, Phys. Rev. D **83**, 114049 (2011).
[72] J.-L. Agram, J. Andrea, E. Conte, B. Fuks, D. Gelé, and P. Lansonneur, Probing top anomalous couplings at the LHC with trilepton signatures in the single top mode, Phys. Lett. B **725**, 123 (2013).
[73] Y.-B. Liu and S. Moretti, Probing tqZ anomalous couplings in the trilepton signal at the HL-LHC, HE-LHC and FCC-hh, Chin. Phys. C **45**, 043110 (2021).
[74] Y.-C. Guo, C.-X. Yue, and S. Yang, Search for anomalous couplings via single top quark production in association with a photon at LHC, Eur. Phys. J. C **76**, 596 (2016).
[75] T. Han, R. D. Peccei, and X. Zhang, Top quark decay via flavor changing neutral currents at hadron colliders, Nucl. Phys. **B454**, 527 (1995).
[76] D. Stolarski and A. Tonero, Constraining new physics with single top production at LHC, J. High Energy Phys. 08 (2020) 036.
[77] J. A. Aguilar-Saavedra, Effective four-fermion operators in top physics: A Roadmap, Nucl. Phys. **B843**, 638 (2011); Erratum, Nucl. Phys. **B851**, 443 (2011).
[78] J. Campbell, R. K. Ellis, and R. Röntsch, Single top production in association with a Z boson at the LHC, Phys. Rev. D **87**, 114006 (2013).
[79] D. Pagani, I. Tsinikos, and E. Vryonidou, NLO QCD + EW predictions for $tHj$ and $tZj$ production at the LHC, J. High Energy Phys. 08 (2020) 082.
[80] A. Giammanco and R. Schwienhorst, Single top-quark production at the Tevatron and the LHC, Rev. Mod. Phys. **90**, 035001 (2018).
[81] C. Escobar, SM and BSM physics in single top quark at the LHC, in *Proceedings of 5th Large Hadron Collider Physics Conference* (2017) [arXiv:1709.02749].
[82] A. Giammanco, Single top quark production at the LHC, Rev. Phys. **1**, 1 (2016).
[83] M. Aaboud *et al.*, Measurement of the production cross section of a single top quark in association with a Z boson in proton–proton collisions at 13 TeV with the ATLAS detector, Phys. Lett. B **780**, 557 (2018).
[84] G. Aad *et al.*, Observation of the associated production of a top quark and a $Z$ boson in $pp$ collisions at $\sqrt{s} = 13$ TeV with the ATLAS detector, J. High Energy Phys. 07 (2020) 124.
[85] A. M. Sirunyan *et al.*, Measurement of the associated production of a single top quark and a Z boson in pp collisions at $\sqrt{s} = 13$ TeV, Phys. Lett. B **779**, 358 (2018).
[86] A. M. Sirunyan *et al.*, Observation of Single Top Quark Production in Association with a $Z$ Boson in Proton-Proton Collisions at $\sqrt{s} = 13$ TeV, Phys. Rev. Lett. **122**, 132003 (2019).
[87] A. M. Sirunyan *et al.*, Search for new physics in top quark production with additional leptons in proton-proton collisions at $\sqrt{s} = 13$ TeV using effective field theory, J. High Energy Phys. 03 (2021) 095.
[88] W. Buchmuller and D. Wyler, Effective Lagrangian analysis of new interactions and flavor conservation, Nucl. Phys. **B268**, 621 (1986).
[89] C. Arzt, M. B. Einhorn, and J. Wudka, Patterns of deviation from the standard model, Nucl. Phys. **B433**, 41 (1995).
[90] M. B. Einhorn and J. Wudka, The bases of effective field theories, Nucl. Phys. **B876**, 556 (2013).
[91] B. Grzadkowski, M. Iskrzynski, M. Misiak, and J. Rosiek, Dimension-six terms in the standard model Lagrangian, J. High Energy Phys. 10 (2010) 085.

[92] I. Brivio and M. Trott, The standard model as an effective field theory, Phys. Rep. **793**, 1 (2019).
[93] S. Bar-Shalom and J. Wudka, Flavor changing single top quark production channels at $e+$ $e-$ colliders in the effective Lagrangian description, Phys. Rev. D **60**, 094016 (1999).
[94] B. Grzadkowski, Four Fermi effective operators at $e^+e^- \to \bar{t}t$, Acta Phys. Pol. B **27**, 921 (1996), arXiv:hep-ph/9511279.
[95] B. Grzadkowski, Z. Hioki, and M. Szafranski, Four Fermi effective operators in top quark production and decay, Phys. Rev. D **58**, 035002 (1998).
[96] J. Abdallah *et al.*, Search for single top quark production via contact interactions at LEP2, Eur. Phys. J. C **71**, 1555 (2011).
[97] P. Achard *et al.*, Search for single top production at LEP, Phys. Lett. B **549**, 290 (2002).
[98] M. Tanaka and R. Watanabe, New physics in the weak interaction of $\bar{B} \to D^{(*)}\tau\bar{\nu}$, Phys. Rev. D **87**, 034028 (2013).
[99] I. Doršner, S. Fajfer, N. Košnik, and I. Nišandžić, Minimally flavored colored scalar in $\bar{B} \to D^{(*)}\tau\bar{\nu}$ and the mass matrices constraints, J. High Energy Phys. 11 (2013) 084.
[100] Y. Sakaki, M. Tanaka, A. Tayduganov, and R. Watanabe, Testing leptoquark models in $\bar{B} \to D^{(*)}\tau\bar{\nu}$, Phys. Rev. D **88**, 094012 (2013).
[101] S. Sahoo and R. Mohanta, Scalar leptoquarks and the rare $B$ meson decays, Phys. Rev. D **91**, 094019 (2015).
[102] C.-H. Chen, T. Nomura, and H. Okada, Explanation of $B \to K^{(*)}\ell^+\ell^-$ and muon $g-2$, and implications at the LHC, Phys. Rev. D **94**, 115005 (2016).
[103] U. K. Dey, D. Kar, M. Mitra, M. Spannowsky, and A. C. Vincent, Searching for leptoquarks at IceCube and the LHC, Phys. Rev. D **98**, 035014 (2018).
[104] D. Bečirević and O. Sumensari, A leptoquark model to accommodate $R_K^{\rm exp} < R_K^{\rm SM}$ and $R_{K^*}^{\rm exp} < R_{K^*}^{\rm SM}$, J. High Energy Phys. 08 (2017) 104.
[105] O. Popov, M. A. Schmidt, and G. White, $R_2$ as a single leptoquark solution to $R_{D^{(*)}}$ and $R_{K^{(*)}}$, Phys. Rev. D **100**, 035028 (2019).
[106] R. Barbieri, G. Isidori, A. Pattori, and F. Senia, Anomalies in $B$-decays and $U(2)$ flavour symmetry, Eur. Phys. J. C **76**, 67 (2016).
[107] R. Alonso, B. Grinstein, and J. Martin Camalich, Lepton universality violation and lepton flavor conservation in $B$-meson decays, J. High Energy Phys. 10 (2015) 184.
[108] D. Buttazzo, A. Greljo, G. Isidori, and D. Marzocca, B-physics anomalies: A guide to combined explanations, J. High Energy Phys. 11 (2017) 044.
[109] L. Di Luzio, A. Greljo, and M. Nardecchia, Gauge leptoquark as the origin of B-physics anomalies, Phys. Rev. D **96**, 115011 (2017).
[110] A. Crivellin, C. Greub, D. Müller, and F. Saturnino, Importance of Loop Effects in Explaining the Accumulated Evidence for New Physics in B Decays with a Vector Leptoquark, Phys. Rev. Lett. **122**, 011805 (2019).
[111] M. J. Baker, J. Fuentes-Martín, G. Isidori, and M. König, High- $p_T$ signatures in vector–leptoquark models, Eur. Phys. J. C **79**, 334 (2019).
[112] I. Doršner, S. Fajfer, A. Greljo, J. F. Kamenik, and N. Košnik, Physics of leptoquarks in precision experiments and at particle colliders, Phys. Rep. **641**, 1 (2016).
[113] V. Gherardi, D. Marzocca, M. Nardecchia, and A. Romanino, Rank-one flavor violation and B-meson anomalies, J. High Energy Phys. 10 (2019) 112.
[114] R. Boughezal, C.-Y. Chen, F. Petriello, and D. Wiegand, Top quark decay at next-to-leading order in the Standard Model effective field theory, Phys. Rev. D **100**, 056023 (2019).
[115] W. Altmannshofer, P. S. Bhupal Dev, and A. Soni, $R_{D^{(*)}}$ anomaly: A possible hint for natural supersymmetry with $R$-parity violation, Phys. Rev. D **96**, 095010 (2017).
[116] Y. Afik, J. Cohen, E. Gozani, E. Kajomovitz, and Y. Rozen, Establishing a search for $b \to s\ell^+\ell^-$ anomalies at the LHC, J. High Energy Phys. 08 (2018) 056.
[117] Y. Afik, S. Bar-Shalom, J. Cohen, and Y. Rozen, Searching for new physics with $b\bar{b}\ell^+\ell^-$ contact interactions, Phys. Lett. B **807**, 135541 (2020).
[118] W. Altmannshofer, P. S. Bhupal Dev, A. Soni, and Y. Sui, Addressing $R_{D^{(*)}}$, $R_{K^{(*)}}$, muon $g-2$ and ANITA anomalies in a minimal $R$-parity violating supersymmetric framework, Phys. Rev. D **102**, 015031 (2020).
[119] Y. Afik, S. Bar-Shalom, J. Cohen, A. Soni, and J. Wudka, High $p_T$ correlated tests of lepton universality in lepton(s) + jet(s) processes; an EFT analysis, Phys. Lett. B **811**, 135908 (2020).
[120] A. Greljo and D. Marzocca, High-$p_T$ dilepton tails and flavor physics, Eur. Phys. J. C **77**, 548 (2017).
[121] D. Marzocca, U. Min, and M. Son, Bottom-flavored Mono-Tau tails at the LHC, J. High Energy Phys. 12 (2020) 035.
[122] D. A. Faroughy, A. Greljo, and J. F. Kamenik, Confronting lepton flavor universality violation in B decays with high-$p_T$ tau lepton searches at LHC, Phys. Lett. B **764**, 126 (2017).
[123] M. Bordone, C. Cornella, J. Fuentes-Martín, and G. Isidori, Low-energy signatures of the $\mathrm{PS}^3$ model: From $B$-physics anomalies to LFV, J. High Energy Phys. 10 (2018) 148.
[124] J. F. Kamenik, A. Katz, and D. Stolarski, On lepton flavor universality in top quark decays, J. High Energy Phys. 01 (2019) 032.
[125] J. E. Camargo-Molina, A. Celis, and D. A. Faroughy, Anomalies in bottom from new physics in top, Phys. Lett. B **784**, 284 (2018).
[126] D. London, P. Saha, and R. Watanabe, B-sector anomalies—The top connection, Springer Proc. Phys. **234**, 401 (2019).
[127] J. Alwall, M. Herquet, F. Maltoni, O. Mattelaer, and T. Stelzer, MADGRAPH5: Going beyond, J. High Energy Phys. 06 (2011) 128.
[128] A. Alloul, N. D. Christensen, C. Degrande, C. Duhr, and B. Fuks, FeynRules2.0—A complete toolbox for tree-level phenomenology, Comput. Phys. Commun. **185**, 2250 (2014).
[129] A. D. Martin, W. J. Stirling, R. S. Thorne, and G. Watt, Parton distributions for the LHC, Eur. Phys. J. C **63**, 189 (2009).

[130] E. Conte, B. Fuks, and G. Serret, MadAnalysis 5, A user-friendly framework for collider phenomenology, Comput. Phys. Commun. **184**, 222 (2013).

[131] The ATLAS Collaboration, Search for trilepton resonances from chargino and neutralino pair production in $\sqrt{s} =$ 13 TeV $pp$ collisions with the ATLAS detector, Report No. ATLAS-CONF-2020-009, 2020.

[132] A. M. Sirunyan *et al.*, Search for Heavy Neutral Leptons in Events with Three Charged Leptons in Proton-Proton Collisions at $\sqrt{s} = 13$ TeV, Phys. Rev. Lett. **120**, 221801 (2018).

[133] S. Mrenna and P. Skands, Automated parton-shower variations in PYTHIA8, Phys. Rev. D **94**, 074005 (2016).

[134] R. D. Ball *et al.*, Parton distributions for the LHC Run II, J. High Energy Phys. 04 (2015) 040.

[135] J. Butterworth *et al.*, PDF4LHC recommendations for LHC Run II, J. Phys. G **43**, 023001 (2016).

[136] M. L. Mangano, M. Moretti, F. Piccinini, and M. Treccani, Matching matrix elements and shower evolution for top-quark production in hadronic collisions, J. High Energy Phys. 01 (2007) 013.

[137] J. de Favereau, C. Delaere, P. Demin, A. Giammanco, V. Lemaître, A. Mertens, and M. Selvaggi, DELPHES3, A modular framework for fast simulation of a generic collider experiment, J. High Energy Phys. 02 (2014) 057.

[138] M. Cacciari, G. P. Salam, and G. Soyez, The anti-$k_t$ jet clustering algorithm, J. High Energy Phys. 04 (2008) 063.

[139] M. Cacciari, G. P. Salam, and G. Soyez, FastJet user manual, Eur. Phys. J. C **72**, 1896 (2012).

[140] M. Cacciari and G. P. Salam, Dispelling the $N^3$ myth for the $k_t$ jet-finder, Phys. Lett. B **641**, 57 (2006).

[141] The ATLAS Collaboration, Expected performance of the ATLAS $b$-tagging algorithms in Run-2, Technical Report No. ATL-PHYS-PUB-2015-022, CERN, Geneva, 2015.

[142] W. Verkerke and D. P. Kirkby, The RooFit toolkit for data modeling, eConf **C0303241**, MOLT007 (2003), arXiv:physics/0306116.

[143] A. L. Read, Presentation of search results: The CL(s) technique, J. Phys. G **28**, 2693 (2002).

[144] P. Azzi *et al.*, Report from Working Group 1: Standard model physics at the HL-LHC and HE-LHC, CERN Yellow Rep. Monogr. **7**, 1 (2019), arXiv:1902.04070.

[145] M. L. Mangano *et al.*, Physics at a 100 TeV pp collider: Standard model processes, CERN Yellow Rep. **3**, 1 (2017), arXiv:1607.01831.

[146] M. Dong *et al.*, CEPC conceptual design report: Volume 2—Physics & detector, arXiv:1811.10545.

[147] R. Franceschini *et al.*, The CLIC potential for new physics, CERN Yellow Rep. Monogr. **3** (2018), https://doi.org/10.23731/CYRM-2018-003.

[148] J. L. Abelleira Fernandez *et al.*, A large hadron electron collider at CERN: Report on the physics and design concepts for machine and detector, J. Phys. G **39**, 075001 (2012).

[149] L. Shi and C. Zhang, Probing the top quark flavor-changing couplings at CEPC, Chin. Phys. C **43**, 113104 (2019).

[150] W. Liu and H. Sun, Top FCNC interactions through dimension six four-fermion operators at the electron proton collider, Phys. Rev. D **100**, 015011 (2019).